

# Planetary Tides and Elastic Response

## From Theory to Calculations

Deivy J. Mercado R.



# Planetary Tides and Elastic Response

From Theory to Calculations

This is a thesis submitted in partial fulfilment  
of the requirements for the degree in

Astronomy

Author:

Deivy J. Mercado R.

Supervisor:

Dr. Jorge I. Zuluaga C.

Second supervisor:

Dra. Gloria A. Moncayo G.

Affiliation:

Physics Institute

Date:

January, 2026

Cover image:

Man in Moon by Dani Caxete

Template style:

Thesis style by Richelle F. van Capelleveen

Template licence:

Licenced under CC BY-NC-SA 4.0



UNIVERSIDAD  
DE ANTIOQUIA

Calle 70 No. 52 – 21 Medellín, Colombia

# Abstract

Tides encode information about the structure, composition and evolution of planetary systems. This thesis develops a coherent pathway from the fundamentals of tidal potential theory and elasticity to practical computations of tidal signals and elastic responses. We review and derive the Tide-Generating Potentials (TGP<sub>s</sub>) in spherical-harmonic form, the governing elastodynamic equations for a self-gravitating, elastic, transversely isotropic, spherical body, and the coupled first-order Ordinary Differential Equations (ODEs) that define the displacement, strain, stress, and perturbing potential fields, to study the planet's response. The resulting framework is implemented in *TSPICE*, a Python package that uses SPICE's kernels and modular routines to compute tidal signals and integrate planetary interior models. We reproduce tidal signals on Earth consistent with the ETERNA-x signal and tidal spectrum. Using a modified PREM Earth model, we compute degree-2 and degree-3 Love numbers at the  $M_2$  tidal frequency, yielding values in good agreement with the previous literature. We explain how *TSPICE* works and which classes provide the functionality for the calculations, giving examples of how to use it in Python scripts. The thesis outlines extensions to alternative interior models, additional bodies, and future work on geophysical inversions, viscoelastic regimes, and new integration setups to enable broader applications in planetary and Earth sciences.

# Acknowledgements

This part is reserved for the acknowledgements.

# Contents

<b>Abstract .....</b>	iii
<b>Acknowledgements .....</b>	iv
<b>List of Tables .....</b>	vii
<b>List of Figures .....</b>	viii
<b>Nomenclature .....</b>	ix
<b>1 Introduction .....</b>	1
<b>2 Tides .....</b>	4
2.1 Tidal Force	4
2.2 Tidal Potential	7
2.3 Potential in Geographic Coordinates	10
2.4 Direct calculation	12
2.5 Harmonic decomposition	13
2.6 Derivatives of the potential	15
<b>3 Elasticity theory .....</b>	18
3.1 Strain tensor	18
3.2 Stress tensor	21
3.3 Equation of motion	24
3.4 Stress-strain relation	27
<b>4 Planetary response .....</b>	32
4.1 Spheroidal oscillations	32
4.2 Love numbers	33

4.3	Spheroidal strain, stress and potential	34
4.4	Differential equations for the elastic response	36
4.5	Boundary conditions	39
4.6	Solutions at the centre	41
<b>5</b>	<b>Calculations .....</b>	<b>44</b>
5.1	Tidal Potential Calculations	44
5.1.1	Calculation routine .....	45
5.1.2	Tides on the Earth .....	47
5.1.3	Tides on the Moon .....	48
5.1.4	Tides on Io .....	49
5.2	Love numbers Calculations	53
5.2.1	Integration setup .....	53
5.2.2	Love numbers for the Earth .....	61
5.3	TSPICE: Tidal Signal with Python and SPICE	61
5.3.1	Body class .....	62
5.3.2	BodyResponse class .....	63
5.3.3	Examples .....	64
<b>6</b>	<b>Analysis &amp; Future Work .....</b>	<b>66</b>
<b>7</b>	<b>Conclusions .....</b>	<b>67</b>
<b>A</b>	<b>Appendix: SPICE .....</b>	<b>68</b>
	<b>Bibliography .....</b>	<b>69</b>

# List of Tables

2.1	Comparison of the term $GM_{\text{ext}}/r^3$ in the Earth tides for different bodies .....	9
5.1	Comparison of Love numbers for the Earth at the $M_2$ tidal frequency	61

# List of Figures

2.1	Configuration of the system to calculate the tidal force .....	5
2.2	Tidal force field generated by an external body on a spherical body ..	6
2.3	Convergence of the factor $(a/r)^n$ for the Earth's tides using different external bodies .....	9
2.4	Tide-generating potential signal on Earth due to the Moon .....	12
2.5	Tide-generating potential signal on Earth due to the Moon, Sun and the planets .....	14
2.6	Spectrum of the tide-generating potential on Earth computed with TSPICE .....	15
3.1	Explanation of strain with material vectors .....	19
3.2	Force acting on a plane that passes through the point $O$ inside the body .....	21
3.3	Visualization of components of the stress tensor .....	23
5.1	Comparison of the tide-generating potential signal obtained with TSPICE and the perturbing potential retrieved with ETERNA-x .....	48
5.2	Spectrum of the tide-generating potential on Earth computed with ETERNA-X .....	49
5.3	Spatial and temporal evolution of the tide-generating potential on the Earth's surface .....	50
5.4	Tide-generating potential and frequency spectrum for the Moon's tides .....	51
5.5	Tide-generating potential and frequency spectrum for Io's tides ..	52
5.6	Planetary profiles from the modified PREM .....	54
5.7	Integration of the functions $y_i(r)$ through the Earth's inner core ..	56
5.8	Integration of the functions $z_i(r)$ through the Earth's outer core ..	58
5.9	Integration of the functions $y_i(r)$ through the Earth's mantle and crust	60

# Nomenclature

## Acronyms

Notation	Description	Page List
CMB	Core-Mantle Boundary	53, 54, 57–60
COM	Center of Mass	5–8, 11, 44
ET	Ephemeris Time	46, 62
ICB	Inner Core Boundary	53, 54, 56, 58
ODE	Ordinary Differential Equation	iii, 2, 32, 36–38, 41, 44, 53, 55, 57–61, 63, 64
PREM	Preliminary Reference Earth Model	53–59, 61
SS	Solar System	1, 2, 13, 14, 44, 49

Notation	Description	Page List
TGP	Tide-Generating Potential	iii, 7, 8, 10–15, 17, 18, 26, 27, 32, 33, 40, 44, 47, 48, 50–53, 62, 64
UTC	Coordinated Universal Time	46, 62

## Constants

Notation	Description	Unit
$G$	Gravitational constant	$6.674 \times 10^{-11} \text{ m}^3 \text{ kg}^{-1} \text{ s}^{-2}$

## Units

Notation	Description	Unit
AU	Astronomical unit	$1.496 \times 10^{11} \text{ m}$
$g_{\oplus}$	Earth's standard gravity	$9.81 \text{ m s}^{-2}$
$M_{\oplus}$	Earth mass	$5.972 \times 10^{24} \text{ kg}$
$M_J$	Jupiter mass	$1.898 \times 10^{27} \text{ kg}$
$M_{\odot}$	Solar mass	$1.988 \times 10^{30} \text{ kg}$
$R_{\oplus}$	Earth mean radius	$6.378 \times 10^6 \text{ m}$
$R_J$	Jupiter mean radius	$7.149 \times 10^7 \text{ m}$
$R_{\odot}$	Solar radius	$6.957 \times 10^8 \text{ m}$

# 1 . Introduction

Pierre-Simon Laplace, one of the most important astronomers and mathematicians in history, once remarked that the problem of tides ranks among “the most complex and interesting problems of the whole physical astronomy” (De Paris et al., 2013). Indeed, the study of tides remains central to our understanding of the origin, evolution, and composition of planetary systems, and it shapes diverse phenomena across the universe and within our own Solar System (SS).

Tidal interactions manifest in a variety of striking ways in planetary science. One dramatic example is *tidal disruption*, in which celestial bodies approach the Roche limit and tidal forces disrupt them, shaping the formation of planetary rings and influencing the planet formation process itself. Particularly relevant for exoplanets in close-in orbits and for many moons in our SS are *tidal locking* situations, in which a body’s rotational period matches its orbital period. *Tidal dissipation*, whereby internal friction generated by a differentiated response to deformation across different parts of a body produces heat, plays a crucial role in the geology and potential habitability of moons and planets, as seen in the subsurface oceans of Europa and the volcanic activity on Io. Furthermore, tidal interactions are responsible for the gradual migration of planets and moons through angular momentum exchange over astronomical timescales.

Beyond planetary science, even, tides are of profound importance across other areas of astrophysics. In compact binary systems, tidal forces influence the evolution of neutron stars and black holes, thereby affecting their gravitational-wave emissions. Galactic dynamics are likewise shaped by tidal encounters, with interactions between galaxies producing tidal tails and triggering episodes of star formation. In stellar astrophysics, tides can alter the rotational and internal dynamics of stars in binary systems, with far-reaching implications for their life cycles. Just to mention a few examples.

The most compelling problems related to tides in this work stem from recent advances and open questions. For instance, could the tidal response be used to infer the planets’ interior structures? What can tides reveal about an exoplanet’s mass distribution and composition? Beyond the centrifugal forces arising from rotation, planetary shapes are also sculpted by tidal forces. More precisely, this depends on how much the body responds to these forces. Various observational techniques have been proposed to measure these responses, in extreme situations, such as exoplanets very close to their host stars (e.g., the hot Jupiter

WASP-12b), as well as in less extreme cases, such as the giant planets in our SS affected by the tidal potential generated by their natural satellites. If successfully achieved, these measurements can constrain the planets' mass distribution, an open problem in planetary science. We suggest the review by Lainey et al. (2025) on quantifying tides on giant planets, and the study by van Dijk & Miguel (2025) that presents a method for retrieving exoplanets' interior properties using Love number measurements.

For rocky exoplanets, understanding the mass distribution is essential because composition and internal structure are first-order controls on a planet's habitability. For instance, the planet's dynamic state, including the viability of plate tectonics and the longevity of a magnetic field, is dictated by its internal heat budget and core-mantle structure. However, characterising these interiors remains a significant challenge, as the main observational techniques provide only two parameters: mass and radius. This creates a degeneracy in which multiple internal compositions and structures can produce the same observed mass and radius measurements Unterborn et al. (2016). By studying planetary tides and, when possible, the resulting elastic response, we may introduce additional constraints into models, thereby helping to reduce this structural degeneracy and enabling a more accurate characterisation of a planet's true interior state.

Another special motivation came from the tidal triggering of earthquakes. Could tidal stresses really trigger seismic events on Earth? An increasing number of studies show that seismic events are positively correlated with tidal forces across different geological settings (e.g., tectonic and volcanic environments), particularly for major global earthquakes (magnitude > 7). Although tidal stresses are small compared with tectonic stresses, tidal forces are considered the "final catalyst" that could trigger earthquakes when the fault is already in a critical state. Nevertheless, contradictory results from some studies and the complexity of seismic activity make this an open problem with no "definitive answer" (Yan et al., 2023; Varga & Grafarend, 2018). Mathematical and computational models of tides could help explain these discrepancies and broaden our understanding of the subject.

These problems motivate this thesis to provide a specialised review of the theory of tidal potentials and planetary response, with a focus on the elastic regime. We include all the mathematical and physical foundations required for key calculations, and therefore consider this an important work that will guide future developments and research.

The structure of this thesis reflects this goal. Following this introduction, the second chapter presents the basic theory of tides and the tidal potential. The third chapter reviews the theory of elasticity, emphasising the mathematical and physical principles essential for describing planetary responses. In the fourth chapter, we derive and discuss the ODEs governing elastic planetary displacements, strain, stress, and the perturbing potential. The fifth chapter is devoted to practical applications: we compute tidal potentials and planetary responses, and introduce *TSPICE*, a Python package developed for these computations and intended to facilitate future research. The sixth chapter analyses and discusses

the results obtained and offers perspectives on improving and extending TSPICE in planetary and Earth sciences research. Finally, the seventh chapter presents our main conclusions.

It is worth noting that this thesis does not follow a conventional structure. The need for a more extensive theoretical review of the foundations, compared with previous literature in the subject, has led to an organisation that departs from standard practice. Nevertheless, the first four chapters may be regarded as the theoretical framework, the fifth as a combined methodology and results section, the sixth as analysis, and the seventh as conclusions. This structure aims to provide both a comprehensive foundation and a practical path forward for research into planetary tides and their elastic response.

# 2 . Tides

Tides occur in nature as a consequence of the difference in the gravitational force exerted by an external body over an extended target body. In the physical world, the planetary bodies are not the ideal points that concentrate all the mass, as in many approximations of celestial mechanics. The extension of the planets causes some parts closer to the external body to feel a stronger gravitational force, while the farther parts feel a weaker attraction. *This difference in the gravitational force is what gave rise to tides.* Mathematically, we can infer that this concept should be related in some way to the derivative of the force in space. This brief explanation, proposed by some authors (Tokieda, 2013; Agnew, 2015), enables us to begin studying the tides in detail.

In the following sections, we will review some useful expressions related to the tidal force (section 2.1) and the tidal potential (section 2.2). For simplicity, we can assume that the Earth is the target body, even though this can be generalised to any planetary body. Naturally, the target body depends on our scientific research goal. If our goal were to study the tidal effects on the Moon, the Moon would be our preferred target body. However, if we want to study the correlation between the lunisolar tides and terrestrial seismicity, Earth should be the target body. Similarly, although we will account for the contribution of any celestial body when calculating the tidal potential on the target body, we can use the Moon as a very frequent example.

We will study how to calculate the tidal potential at any point and time on a planetary surface or in its interior (we will discuss the expressions needed in section 2.2, and we will compute them in section 5.1 of chapter 5). This will be useful for calculating planetary deformation and stress (we will explain how they are related in chapter 4). Essentially, this chapter moves from a basic explanation of what the tides are and the mathematical expressions that describe them to how to calculate the tidal signal and its components.

## 2.1 Tidal Force

As we suggested previously, *tidal forces* arise from the gravitational attraction of external bodies on a planetary body. Calculating these forces requires only a basic understanding of potential theory and celestial mechanics. However,

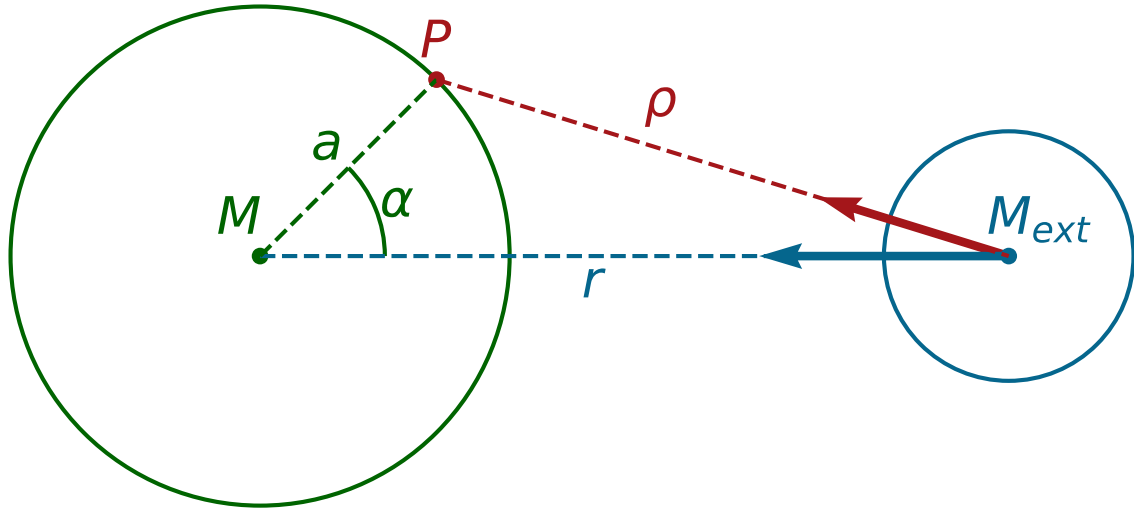


**Figure 2.1:** Configuration of the system to define equation (2.1). Conveniently, we draw the point  $P$  on the body's surface, but equation (2.1) remains valid in the interior. Also, note how the directions of the vectors  $\vec{r}$  and  $\vec{\rho}$  are defined; hence  $\vec{g}_P$  and  $\vec{g}_{\text{orb}}$  point in the opposite directions to these vectors.

these calculations traditionally report accelerations (or specific forces) rather than forces. In this sense, the tidal force at a point  $P$  on or inside the body is defined as the difference between the acceleration caused by an external body at that point,  $\vec{g}_P$ , and the orbital acceleration,  $\vec{g}_{\text{orb}}$ , the acceleration experienced by the body as a whole in its orbit (Agnew, 2015). Mathematically, we can write this definition as:

$$\vec{g}_{\text{tid}} = \vec{g}_P - \vec{g}_{\text{orb}} = -\frac{GM_{\text{ext}}}{\rho^3}\vec{\rho} + \frac{GM_{\text{ext}}}{r^3}\vec{r} \quad (2.1)$$

Where  $G$  is the gravitational constant,  $M_{\text{ext}}$  is the mass of the external body (for instance, Moon, Sun, Jupiter, or any other body), and  $r$  and  $\rho$  are the distances from the planets' Center of Mass (COM) to the external body's COM and to the point  $P$ , respectively. This configuration is illustrated in Figure 2.1, where you can also find the distance  $a$  from the planets' COM to the point  $P$ , and the geocentric angle  $\alpha$  between the position vector of the external body's COM and the position vector of the point  $P$ .

Equation (2.1) is not the formula we will use to derive the tidal signal. However, it remains important because it helps us to initially understand the distribution of tidal forces on a planetary body. Assuming that the Moon is on the right side of our perfectly spherical Earth (as shown in Figure 2.1), and using equation (2.1), we plotted the tidal force field observed in Figure 2.2. In this plot, as in the mathematical expression, we observe that the tidal force is zero at the Earth's COM, because  $\vec{r}$  and  $\vec{\rho}$  are equal there. But there are other interesting insights. In Figure 2.2, all the arrows have been scaled firstly by Earth's average surface

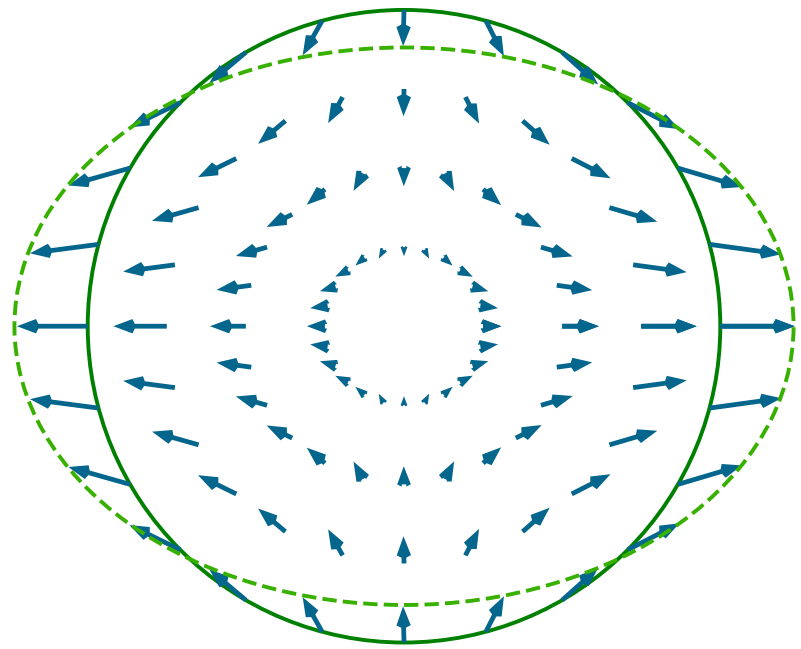


**Figure 2.2:** A static picture of the tidal force field on a spherical body, as defined by equation (2.1). We assume the external body responsible for the field is on the right side of the picture, as in Figure 2.1.

gravity ( $g$ ), and then, with a sufficiently large value to make them visible, since their magnitudes are around one part per million of  $g$ . This allows us to use the size of the arrows to make some physical statements. For instance, the tidal forces increase with distance from the COM, as shown by the larger arrows at a greater radius. Additionally, the tidal force field for our spherically symmetric Earth appears symmetric with respect to the COM. Lastly, we drew an ellipse connecting the heads of the arrows in Figure 2.2 to illustrate the effect of tidal forces on the planet's shape (similar to Agnew, 2015): compressing in the direction perpendicular to the line connecting the bodies, and stretching along the line.

In a real scenario, the vectors  $\vec{r}$  and  $\vec{p}$  vary over time due to the body's orbital motion and rotation, as well as the movement of the external body causing the tides. Consequently, Figure 2.2 is only valid as a static picture, i.e., at a fixed time. Even when the two bodies are in a circular orbit and the magnitude of  $\vec{r}$  remains constant, the tidal force at point  $P$  still varies due to the body's rotation. The planet's rotation moves the vector  $\vec{p}$  around the rotation axis, changing its relative position with respect to the COM. In this case, the tidal signal exhibits only diurnal and semi-diurnal variations. Only in a circular orbit with strict tidal locking of the target body, when rotation and orbital motion are coupled, would the tidal field not change over time. In this scenario, the force field would always be as shown in Figure 2.2.

## 2.2 Tidal Potential

A more common approach to obtain the tidal signal is to determine the TGP and then derive it spatially. To obtain a calculable expression for this potential, we start from the total gravitational potential,  $V_{\text{tot}}$ , at a point  $P$  on the target body due to an external body of mass  $M_{\text{ext}}$  (Agnew, 2015; Simon et al., 2013):

$$V_{\text{tot}} = \frac{GM_{\text{ext}}}{\rho} = \frac{GM_{\text{ext}}}{r} \frac{1}{(1 + (a/r)^2 - 2(a/r) \cos \alpha)^{1/2}} \quad (2.2)$$

In this last expression, we have used the law of cosines to express  $\rho$  in terms of  $a$ ,  $r$  and  $\alpha$ . We also factored out the common distance  $r$ . The term inverse to the square root is similar to the *generating function for Legendre Polynomials*:

$$\sum_{n=0}^{\infty} t^n P_n(x) = \frac{1}{(1 + t^2 - 2xt)^{1/2}} \quad (2.3)$$

Then, if we take  $t = (a/r)$  and  $x = \cos \alpha$ , the potential can be written as:

$$V_{\text{tot}} = \frac{GM_{\text{ext}}}{r} \sum_{n=0}^{\infty} \left(\frac{a}{r}\right)^n P_n(\cos \alpha) \quad (2.4)$$

Equation (2.4) is an important expression, but it represents the total gravitational potential due to  $M_{\text{ext}}$ , not the TGP. It is important to remember that *tides result from gravitational attraction, but are not gravitational attraction itself*. They arise from differences in the gravitational force or potential with respect to the planet's COM. In practice, this means that certain terms must be subtracted from the potential in equation (2.4). Which terms? Those associated with the gravitational attraction felt by the planet as a whole due to its orbit around  $M_{\text{ext}}$ : the potential responsible for the orbital centrifugal acceleration. By expanding  $V_{\text{tot}}$  up to  $n = 2$ , and using the values for  $P_n$  (see definitions in Sepúlveda, 2004), these terms can be readily identified:

$$\begin{aligned} V_{\text{tot}} &= \frac{GM_{\text{ext}}}{R} \left(\frac{a}{r}\right)^0 P_0 + \frac{GM_{\text{ext}}}{r} \left(\frac{a}{r}\right) P_1 + \frac{GM_{\text{ext}}}{r} \sum_{n=2}^{\infty} \left(\frac{a}{r}\right)^n P_n(\cos \alpha) \\ &= \frac{GM_{\text{ext}}}{r} + \frac{GM_{\text{ext}}}{r^2} a \cos \alpha + \frac{GM_{\text{ext}}}{r} \sum_{n=2}^{\infty} \left(\frac{a}{r}\right)^n P_n(\cos \alpha) \end{aligned} \quad (2.5)$$

The first term in this expression is physically irrelevant because it is a constant term and its gradient (spatial derivative) will vanish, hence we can neglect it. On the other hand, the second term is the one that gives us the orbital centrifugal

acceleration. We can prove this by setting  $a \cos \alpha = x$ , the Cartesian coordinate along the vector joining the COM, and by calculating the gradient:

$$\nabla V_{\text{tot},1} = \frac{\partial}{\partial x} \left( \frac{GM_{\text{ext}}}{r^2} x \right) \hat{x} = \frac{GM_{\text{ext}}}{r^2} \hat{x} = -\vec{g}_{\text{orb}} \quad (2.6)$$

In the last step, we used that  $\hat{x} = \hat{r}$  by our definition of this Cartesian coordinate. Finally, removing this term, the expression for the TGP is:

$$V_{\text{tid}}(t) = \frac{GM_{\text{ext}}}{r(t)} \sum_{n=2}^{\infty} \left( \frac{a}{r(t)} \right)^n P_n(\cos \alpha(t)) \quad (2.7)$$

We made explicit the time dependence of  $V_{\text{tid}}$  through  $r$  and  $\alpha$ . However, not all terms in equation (2.7) need to be considered. Given the physical and geometrical interpretation of the argument inside the Legendre Polynomials, we can state that  $|P(\cos \alpha)| \leq 1$ , and, in some very optimistic cases, we can assess how quickly  $(a/r)^n$  converges. For instance, for the Earth, by choosing  $a = a_{\oplus}$  (the tides on the surface) and  $r$  as the minimum possible distance between the Earth, the Moon, the Sun, and the planets, we can see that some terms in the sum contribute very little. As shown in Figure 2.3, the term  $(a_{\oplus}/r)^n$  converges very quickly for most bodies. For this reason, in practice, only terms up to degree  $n = 2$  are usually considered for the Sun and the planets, and up to  $n = 4$  for the Moon, in the case of the Earth tides (Agnew, 2015).

We can also compare the contributions of each planetary body to the tidal signal on Earth for the first degree of the TGP expansion,  $n = 2$ . Assuming that  $a^2 P_2(\cos \alpha)$  is the same for all bodies, we find that:

$$V_{\text{tid}} \propto \frac{GM_{\text{ext}}}{r^3} \quad (2.8)$$

Table 2.1 shows the value of this term for the Earth's tides with respect to different planetary bodies, again taking  $r$  as the minimum possible distance to each body. In this optimistic scenario, which is not far from reality, the Moon is the main contributor to the tidal signal, followed by the Sun, which is farther away but has a much larger gravitational parameter,  $GM_{\text{ext}}$ . Since the Moon's contribution is larger, we also compare the other contributions relative to it. The calculation is consistent with what others have reported (Tokieda, 2013; Simon et al., 2013; Agnew, 2015): the Sun's contribution is almost half that of the Moon. After the Sun, Venus and Jupiter make the next biggest contributions, but these are of the order of parts per million relative to the Moon. This is why, when studying the tides on Earth, it is common to refer to them as *lunisolar tides*, omitting the contribution of the planets. These facts can be used to reduce computing time in calculations.

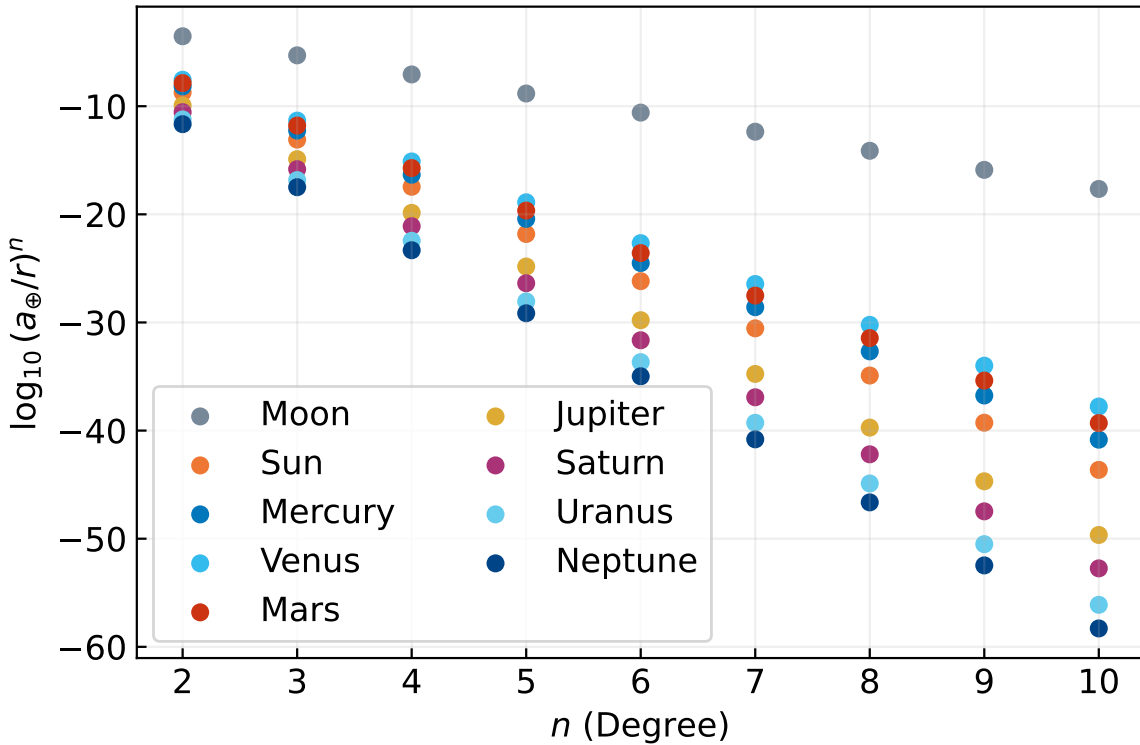


**Figure 2.3:** Convergence of the factor  $(a/r)^n$  for the Earth's tides using different external bodies, with  $a = a_{\oplus}$  (Earth's mean radius) and  $r$  the minimum possible distance between the Earth and the external bodies. We plot the logarithm of this factor because it converges quickly. Due to its distance, the Moon exhibits distinct behaviour compared with the rest of the planets and the Sun.

**Table 2.1:** A comparison of the tidal generating potential term  $GM_{\text{ext}}/r^3$  for various bodies. Values use the minimum Earth-body distance and are shown in both absolute units and normalized to the Moon's value.

Body	$GM_{\text{ext}}/r^3$	
	[ $\text{s}^{-2}$ ]	[Moon fraction]
Moon	$9.59 \times 10^{-14}$	1.0
Sun	$4.17 \times 10^{-14}$	0.435
Mercury	$4.77 \times 10^{-20}$	$4.97 \times 10^{-7}$
Venus	$5.84 \times 10^{-18}$	$6.09 \times 10^{-5}$
Mars	$2.68 \times 10^{-19}$	$2.79 \times 10^{-6}$
Jupiter	$6.22 \times 10^{-19}$	$6.48 \times 10^{-6}$
Saturn	$2.20 \times 10^{-20}$	$2.30 \times 10^{-7}$
Uranus	$3.28 \times 10^{-22}$	$3.42 \times 10^{-9}$
Neptune	$8.56 \times 10^{-23}$	$8.93 \times 10^{-10}$

## 2.3 Potential in Geographic Coordinates

Equation (2.7) for the TGP is expressed in terms of the geocentric angle  $\alpha$ , which represents the angular distance between the point  $P$  on the planet where the tide is being calculated and the subpoint (the projection) of the external body  $M_{\text{ext}}$  onto the planet's surface. While we previously studied the convergence of this expression for the Earth's tides with respect to different bodies, we did not compute the value of the TGP for a specific location on Earth at a particular time. To achieve this calculation, it is preferable to express the angle  $\alpha$  in terms of *geographic coordinates* on the target body using the *law of cosines for spherical triangles*:

$$\cos \alpha = \cos \theta \cos \theta' + \sin \theta \sin \theta' \cos (\phi' - \phi) \quad (2.9)$$

Where,  $\theta$  and  $\phi$  denote the colatitude and longitude of point  $P$  on the planet, respectively, while  $\theta'$  and  $\phi'$  denote the colatitude and longitude of the projection of the external body onto the planet. Inserting the expression for  $\cos \alpha$  into the Legendre Polynomials, together with developments in mathematical physics, yields the *addition theorem for spherical harmonics*:

$$P_n(\cos \alpha) = \frac{4\pi}{2n+1} \sum_{m=-n}^n \bar{Y}_n^m(\theta', \phi') Y_n^m(\theta, \phi) \quad (2.10)$$

Substituting equation (2.10) into the potential yields:

$$V_{\text{tid}}(t) = \frac{GM_{\text{ext}}}{r(t)} \sum_{n=2}^{\infty} \left( \frac{a}{r(t)} \right)^n \frac{4\pi}{2n+1} \sum_{m=-n}^n \bar{Y}_n^m(\theta'(t), \phi'(t)) Y_n^m(\theta, \phi) \quad (2.11)$$

By convention, the TGP is often expressed as  $V_{\text{tid}}/g$ , where  $g$  is a reference gravitational acceleration. For instance, we can assume that  $g$  is the acceleration at the planet's mean radius  $a_p$ :

$$g = \frac{GM}{a_p^2} \quad (2.12)$$

With  $M$  the mass of the planet. When dividing equation (2.11) by  $g$ , we obtain the following expression:

$$\frac{V_{\text{tid}}(t)}{g} = a_p^2 \frac{M_{\text{ext}}}{M} \sum_{n=2}^{\infty} \frac{a^n}{r^{n+1}} \frac{4\pi}{2n+1} \sum_{m=-n}^n \bar{Y}_n^m(\theta'(t), \phi'(t)) Y_n^m(\theta, \phi) \quad (2.13)$$

In addition, we can group some of the constant terms with the distance  $a$  from the COM (similar to Agnew, 2015)<sup>1</sup>:

$$K_n(a) = a_p^2 a^n \frac{M_{\text{ext}}}{M} \frac{4\pi}{2n+1} \quad (2.14)$$

And using this definition of  $K_n$  in the TGP, we obtain the following expression:

$$\frac{V_{\text{tid}}(t)}{g} = \sum_{n=2}^{\infty} \frac{K_n(a)}{r(t)^{n+1}} \sum_{m=-n}^n \bar{Y}_n^m(\theta'(t), \phi'(t)) Y_n^m(\theta, \phi) \quad (2.15)$$

Equation (2.15) is very helpful for calculating tides at any depth on a planet using astronomical tools that determine the positions of celestial bodies over time. However, it may be useful to clarify what the highlighted quantity represents. One way to do this is through dimensional analysis:

$$\left[ \frac{V_{\text{tid}}}{g} \right] = \frac{\text{J/kg}}{\text{m/s}^2} = \frac{\text{m}^2/\text{s}^2}{\text{m/s}^2} = \text{m}$$

Thus,  $V_{\text{tid}}/g$  has units of length or displacement. Since the implied quantity is the potential, this can be interpreted as a height relative to the equipotential surface of the planet's gravitational field. On Earth, this most closely coincides with the mean sea level, the *geoid*. This should not be confused with the amount of movement that the oceans will undergo because of the TGP. Neither is the TGP the total additional gravitational potential. As we will see in chapter 4, the additional potential and the actual displacements on the planet will be fractions of these quantities and will also depend on the planet's structure and composition.

Moreover, we can already observe another property of the TGP in equation (2.7). The value of each component of degree  $n$  in the TGP varies as  $(a/a_p)^n$  as we move towards or away from the COM, which can be shown by manipulating the terms in equation (2.14) slightly:

$$K_n(a) = a_p^{n+2} \frac{M_{\text{ext}}}{M} \frac{4\pi}{2n+1} \left( \frac{a}{a_p} \right)^n = K_n(a_p) \left( \frac{a}{a_p} \right)^n \quad (2.16)$$

Therefore, using equation (2.16) we can also write the potential as follows:

$$\frac{V_{\text{tid}}(t)}{g} = \sum_{n=2}^{\infty} \left( \frac{a}{a_p} \right)^n \frac{K_n(a_p)}{r(t)^{n+1}} \sum_{m=-n}^n \bar{Y}_n^m(\theta'(t), \phi'(t)) Y_n^m(\theta, \phi) \quad (2.17)$$

---

<sup>1</sup>The constant  $K_n$  is similar to that defined by Agnew (2015), but not identical, differing by a factor of  $1/\bar{r}$ . They work with  $\bar{r}$  because the mean distances to other bodies are well known for the Earth. However, our choice of  $K_n$  allows us to have a more general (or programmable) form of the TGP that can easily be extended to other planetary bodies.

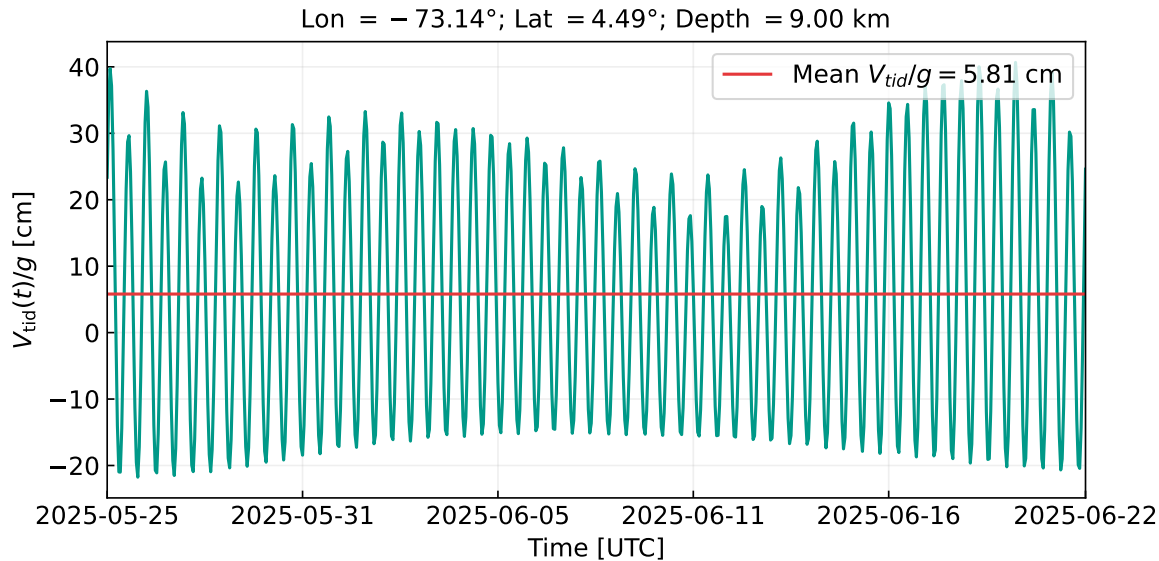


**Figure 2.4:** Tide-generating potential due to the Moon over a specific time window at a specific location on Earth. The potential is given as height above the geoid, and the signal is computed with a time step of 1 hour. The horizontal red line shows the average value of the signal over that period. Computed using the Python package *TSPICE*, which we developed for this work and presented in chapter 5.

For now, we can use either equation (2.15) or equation (2.17) to compute the tidal potential on the Earth or any other planetary body by replacing  $M$  and  $a_p$  with the corresponding mass and mean radius, respectively. This will be our initial approximation of the tidal signal.

## 2.4 Direct calculation

Classically, geophysicists compute the tidal signal on Earth in two ways: using pre-established coefficients from a *harmonic decomposition* of tides, or by explicitly using some of the equations we previously derived for the tidal potential, which require calculating astronomical ephemerides. This last option is called a *direct calculation* of the potential (Agnew, 2015). We will carry out these calculations in section 5.1, where we also explain how we designed *TSPICE*, a Python package to quickly and easily compute the signal using astronomical ephemerides, and how to use it.

As a first test of equation (2.17), we compute the corresponding tidal signal on Earth due to the Moon over a specific time interval and at a particular location. Figure 2.4 shows the tidal potential computed at the coordinates 4.49°N, 73.14°W over a lunar month (from June 25 to July 22, 2025), using terms up to degree  $n = 6$ . This time window isn't astronomically special. We chose this period as an example because it coincides with an earthquake at the location we are using.

Figure 2.4 shows this signal, and it is quickly evident that the semi-diurnal

variations, the shortest visible variations in the signal, occur approximately every half day. Looking closely at the amplitude variation, we may identify a diurnal pattern over a full day. Finally, there are additional variations in the signal over longer periods, as evidenced by the sinusoidal variations that appear, masking all the signal peaks. In general, all these frequencies, corresponding to or around some well-known astronomical ephemerides (the Earth's rotation and the lunar month, for instance), are hidden in the signal; so a complete and more rigorous decomposition of the signal into its fundamental frequencies requires a Fourier analysis, as it will be explained in section 2.5.

Since the potential is linear, contributions from various bodies can be aggregated to obtain a total signal. In geophysical measurements, this approach may be more advantageous than analysing separate signals from individual bodies, which can be difficult to isolate. Figure 2.5 shows the TGP at a specific period and location on Earth due to the Moon, Sun and planets, with each contribution computed up to degree  $n = 6$ . We also show the separate contributions, and, as expected from Table 2.1, the most significant contributions to the Earth tides come from the Moon and the Sun. In terms of the "height above the geoid",  $V_{\text{tid}}/g$ , the Moon and Sun contributions are on the order of centimetres, while the largest planetary contributions are on the order of nanometres.

The examples given here use calculations on Earth because the signal of Earth tides is well known, but we will test our equations with calculations for other bodies in the SS in section 5.1.

## 2.5 Harmonic decomposition

From the Legendre polynomials in equation (2.7), we can already see that the potential can be decomposed into a series of sinusoidal waves with different periods. Laplace introduced the TGP and was also the first to attempt to express the tides in this way, creating the spherical harmonics in the process. This first harmonic decomposition, like subsequent attempts, was purely analytical, relying on basic knowledge of celestial mechanics. However, it laid the foundations for other semi-empirical methods that rely on geophysical observations (Deparis et al., 2013).

After Laplace, various improvements were made to obtain a more precise harmonic expansion. Among these, we count the important contributions of Lord Kelvin (1867), George H. Darwin (1883) and Arthur T. Doodson (1921) (Deparis et al., 2013). The last two even created systems to name and identify the most important frequencies of the Earth tides: the *Darwin symbols* and the *Doodson numbers*. More recent works use more precise analytical ephemerides (as in Cartwright & Tayler, 1971) or numerical ephemerides with thousands of terms in the expansion (as in Hartmann & Wenzel, 1995) to compute the tidal potential directly and then decompose it. Thus, the study of tides, at least for Earth tides, has advanced significantly in the frequency domain (Agnew, 2015).

But what does a tidal spectrum look like? Figure 2.6 shows the spectrum of the tidal signal at the same location on Earth as in Figure 2.5 and Figure 2.4, computed

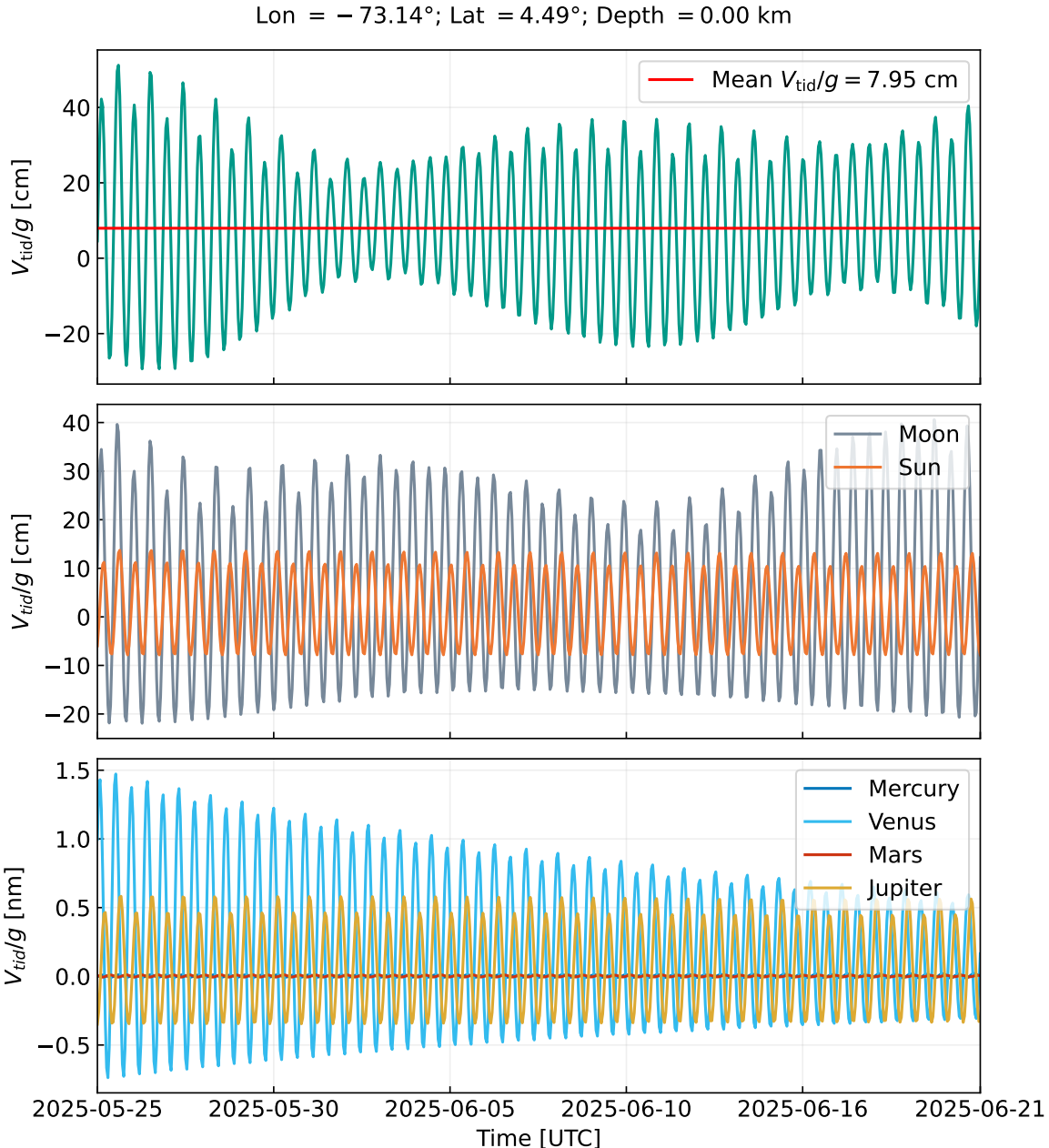


**Figure 2.5:** Tide-generating potential due to the Moon, Sun and planets (Mercury, Venus, Mars and Jupiter) over a specific time window at a specific location on Earth. We chose the same location, time window and step as the signal in Figure 2.4. As in that figure, the potential is given in terms of height above the geoid. The top panel shows the total signal, including contributions from all planetary bodies, with a horizontal red line indicating the average value of this signal over that period. The middle panel shows the Sun and Moon contributions separately; as we can see, they are on the order of centimetres and are the largest. The bottom panel shows only the planets' contribution, which is in nanometres and hence very small. Computed using our package TSPICE, which allows the computation of the contributions from different planetary bodies in the SS.

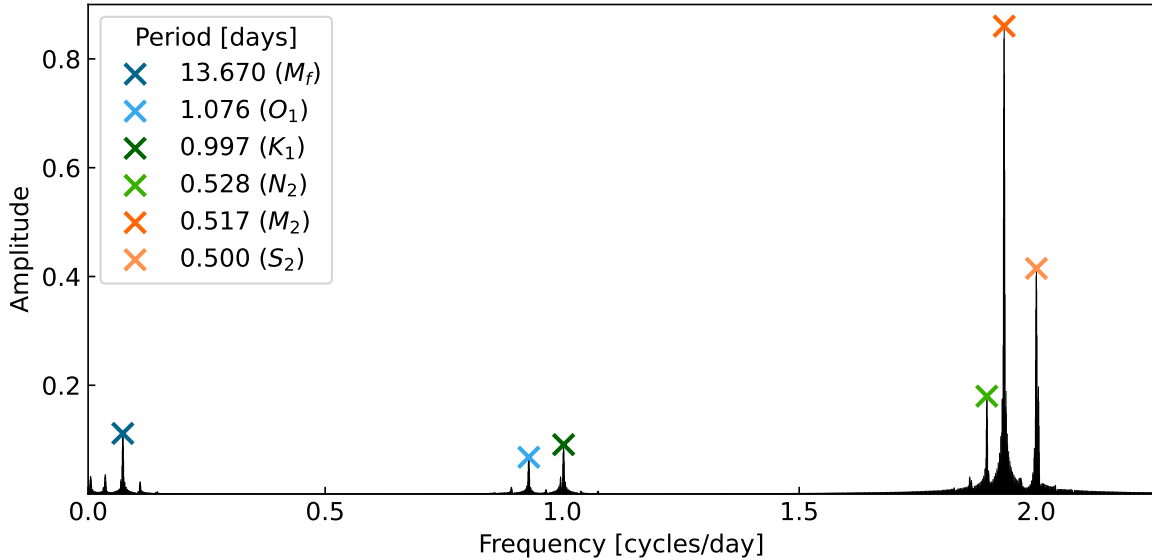


**Figure 2.6:** Spectrum of the tide-generating potential on Earth. The signal was calculated at the same location as in Figure 2.4, but for a complete year. After computing the tidal signal using TSPICE, we used LombScargle from Astropy to determine the frequencies and their corresponding amplitudes. The plot also marks some of the more pronounced peaks. The frequencies of these peaks, in cycles per day, match those of some harmonic components with well-known Darwin symbols. We identified the corresponding periods and Darwin symbols of these peaks in the figure's legend.

over a complete year at 30 min intervals and including contributions from the Moon, Sun and planets. To compute the spectrum, we use the *LombScargle* method (VanderPlas, 2018) from *Astropy* (Astropy Collaboration et al., 2013, 2018, 2022). The amplitude was obtained by taking the square root of the power returned by LombScargle, and we identified the most important frequencies in the spectrum, along with their periods and Darwin symbols.

The spectrum in Figure 2.6 suggests that the signal comprises three main bands: the semi-diurnal band centred on 2 cycles/day with the highest peaks, the diurnal band centred on 1 cycles/day, and the long-period (or low-frequency) band near zero. Nevertheless, we haven't been meticulous about selecting the main frequencies in each band; we've highlighted only a few notable peaks in the plot. Harmonic decomposition isn't a primary goal of this work; rather, we aim to compute the tidal signal directly using computational tools to obtain the ephemerides. However, the tidal spectrum could be an indicator of the quality of our calculations, which is why we mention it here.

## 2.6 Derivatives of the potential

As we will see in chapter 4, to compute a geophysical signal, i.e., not the TGP as shown in Figure 2.4, but the planet's response to that signal in terms of displacements, strain, stress, or perturbing potential, we will need the first and second

partial derivatives of  $V_{\text{tid}}$  on many occasions. Hence, we decided to derive some handy expressions here, using the following mathematical identities (Sepúlveda, 2004):

$$Y_n^m(\theta, \phi) = \sqrt{\frac{2n+1}{4\pi} \frac{(n-m)!}{(n+m)!}} P_n^m(\cos \theta) e^{im\phi} \quad (2.18)$$

$$\sqrt{1-x^2} \frac{dP_n^m(x)}{dx} = \frac{1}{2} [(n+m)(n-m+1)P_n^{m-1}(x) - P_n^{m+1}(x)] \quad (2.19)$$

By the definition in equation (2.18), the spherical harmonics in equation (2.11) can be expressed as the product of an associated Legendre polynomial and an exponential function, allowing us to separate the derivatives with respect to each coordinate. The  $l$ th-order derivatives of the azimuthal part are:

$$\frac{d^l}{d\phi^l} (e^{im\phi}) = (im)^l e^{im\phi} \quad (2.20)$$

Subsequently, the partial azimuthal derivatives of the potential are:

$$\frac{\partial^l V_{\text{tid}}}{\partial \phi^l} = \frac{GM_{\text{ext}}}{r} \sum_{n=2}^{\infty} \left(\frac{a}{r}\right)^n \frac{4\pi}{2n+1} \sum_{m=-n}^n (im)^l Y_n^m(\theta, \phi) \bar{Y}_n^m(\theta', \phi') \quad (2.21)$$

This is exactly the expression in equation (2.11), except for the factor  $(im)^l$ . On the other hand, the derivative of the polar part is:

$$\begin{aligned} \frac{d}{d\theta} (P_n^m(\cos \theta)) &= -\sin \theta \frac{d}{d \cos \theta} (P_n^m(\cos \theta)) \\ &= -\sqrt{1-x^2} \frac{dP_n^m(x)}{dx} \end{aligned} \quad (2.22)$$

Where we set  $x = \cos \theta$  to use the recurrence formula in equation (2.19). This yields the first polar derivative of the potential as:

$$\begin{aligned} \frac{\partial V_{\text{tid}}}{\partial \theta} &= \frac{GM_{\text{ext}}}{r} \sum_{n=2}^{\infty} \left(\frac{a}{r}\right)^n \sum_{m=-n}^n \frac{1}{2} \sqrt{\frac{4\pi}{2n+1} \frac{(n-m)!}{(n+m)!}} \bar{Y}_n^m(\theta', \phi') \\ &\times [P_n^{m+1}(\cos \theta) - (n+m)(n-m+1)P_n^{m-1}(\cos \theta)] e^{im\phi} \end{aligned} \quad (2.23)$$

Using other recurrence relations for the associated Legendre polynomials that we don't give here, and by rederiving this last expression, we can obtain

a second azimuthal derivative. However, we are not going to write it here because of its length and because we barely use it. Finally, combining the results in equation (2.21) and equation (2.23), we write the mixed partial derivative of the potential as:

$$\begin{aligned} \frac{\partial V_{\text{tid}}}{\partial \theta \partial \phi} = & \frac{GM_{\text{ext}}}{r} \sum_{n=2}^{\infty} \left(\frac{a}{r}\right)^n \sum_{m=-n}^n \frac{im}{2} \sqrt{\frac{4\pi}{2n+1} \frac{(n-m)!}{(n+m)!}} \bar{Y}_n^m(\theta', \phi') \\ & \times [P_n^{m+1}(\cos \theta) - (n+m)(n-m+1)P_n^{m-1}(\cos \theta)] e^{im\phi} \end{aligned} \quad (2.24)$$

For now, this is all the set of expressions related to the TGP that we may need if we want to convert the TGP into a measurable signal on a planet.

# 3 . Elasticity theory

Before going deep into how the planetary bodies respond to the TGP, we should remember some fundamental aspects and concepts of elasticity theory that will appear repeatedly in the following deductions and calculations, such as the definitions of stress and strain and their relation as an inseparable pair. Also, we should review the fundamental equation of motion for elastodynamics—the Navier-Cauchy relation—especially its form for a layered, transversely isotropic sphere, as we can consider the planets in the first approach. In the next section, we will use many of the relations of this part to deduce an elastic response of the planets to tidal forces. This section follows developments from Lautrup (2011), Love (1944), and Jaeger et al. (2007), but many other books on elasticity theory or rock mechanics also study these results.

## 3.1 Strain tensor

In the theory of continuous matter, the bodies deform due to *displacements*, the movement of the material particles forming the body from the initial,  $X$ , to the final position,  $x$ , which mathematically can be written as the difference between the  $X$  and  $x$  states:

$$\vec{u} = \vec{x} - \vec{X} \quad (3.1)$$

Displacement can include rotations, translations, and stretches or compressions, but not all of these movements cause the body to deform. A *deformation* is defined by a change in the relative geometry between the body's material particles, the infinitesimal constitutive parts of the body. Therefore, a body can experience displacement without undergoing any deformation. However, if, after the displacement, the angle or distance between two vectors connecting points inside the body changes, then the body has sustained a deformation. The rigid body motion, for instance, strictly speaking, is excluded from the deformation because the angles and distances subtended by the position of two particles in the body don't change.

To conclude on the deformation of a body, the primary mathematical tool is the *gradient of the displacement*. Using the definition of displacement and a

Taylor expansion, Lautrup (2011) shows that, after a displacement, it is possible to express the change in the vector connecting two points inside the body,  $\vec{a}_0$ , or what the author referred to as an infinitesimal “needle”, as follows:

$$\delta\vec{a} \equiv \vec{a} - \vec{a}_0 = (\vec{a} \cdot \nabla)\vec{u} \quad (3.2)$$

Here appears, for the first time, the displacement gradient,  $\nabla\vec{u}$ , associated with the change in the vector  $\vec{a}$ . The panel (a) in Figure 3.1 illustrates the material vector within the body in its original and final positions. Using the equation (3.2), we can also calculate the change in the dot product of two material vectors,  $\vec{a}_0$  and  $\vec{b}_0$ , as shown in the panel (b) of Figure 3.1, which could be a good indicator of deformation due to its dependence on the length and angle between the vectors:

$$\begin{aligned} \delta(\vec{a} \cdot \vec{b}) &\equiv \vec{a} \cdot \vec{b} - \vec{a}_0 \cdot \vec{b} \\ &= (\vec{a} \cdot \nabla)\vec{u} \cdot \vec{b} + (\vec{b} \cdot \nabla)\vec{u} \cdot \vec{a} \end{aligned} \quad (3.3)$$

Or in index notation:

$$\delta(a_i b_i) = (\partial_j u_i + \partial_i u_j) a_i b_j \quad (3.4)$$

Note that the changes in the relative geometry between the vectors  $\vec{a}$  and  $\vec{b}$  appear to be stored in the combination of the displacement gradient. Specifically,

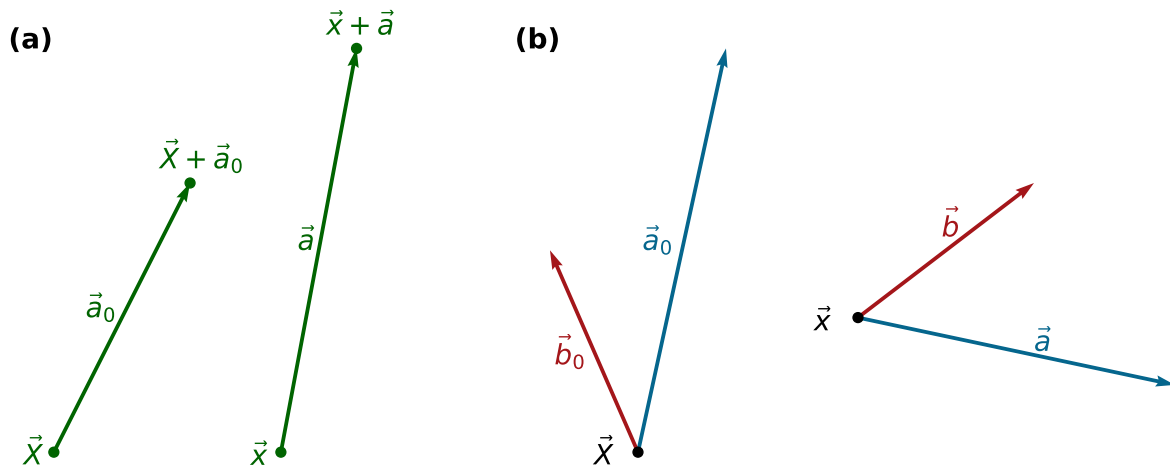


**Figure 3.1:** In panel (a) (left side of the figure), we observe a material vector  $\vec{a}_0$  connecting two points in their initial positions  $\vec{X}$  and  $\vec{X} + \vec{a}_0$ , and their positions  $\vec{x}$  and  $\vec{x} + \vec{a}$  after a displacement. Note that the new vector connecting the points is no longer  $\vec{a}_0$  but  $\vec{a}$ . Equation (3.2) allows us to calculate the change in the material vector connecting the two points. In panel (b) (right side of the figure), we observe two material vectors,  $\vec{a}_0$  and  $\vec{b}_0$ , in their initial positions, at  $\vec{X}$ , and the new material vectors  $\vec{a}$  and  $\vec{b}$ , after displacement, at  $\vec{x}$ . As equation (3.3) suggests, we can analyse the change in the relative geometry between these two vectors through the change in their dot product.

the combination of  $\nabla \vec{u}$  that appears in the last expression allows us to define a new tensor:

$$\boldsymbol{u} = \frac{1}{2}(\nabla \vec{u} + \nabla \vec{u}^T) \quad \text{or} \quad u_{ij} = \frac{1}{2}(\partial_i u_j + \partial_j u_i) \quad (3.5)$$

This is the *Cauchy's (infinitesimal) strain tensor*, or simply the *strain tensor*, as defined by most of the textbooks in the subject. We should point out that this is a symmetric tensor by definition, and each of its components has dimensionless units, which reveal its physical nature as a relative measure of the deformation. Nevertheless, the strain as defined in the equation (3.5) is only applicable for slowly varying displacement fields, that is, fields satisfying the condition (Lautrup, 2011):

$$|\partial_j u_i(x)| \ll 1 \quad (3.6)$$

This is the case in many interesting problems, where changes in the object's size and shape are relatively small compared to its dimensions. We expect that this is also the case for a planet's deformation due to tidal forces, at least in non-extreme gravitational environments. As a result, when this strain tensor is specified at a point in the body, we can precisely account for the strain state at that point. For instance, we can tell how it changed the volume around that point using the trace of  $\boldsymbol{u}$  defined as:

$$\text{tr}(\boldsymbol{u}) = \sum_i \partial_i u_i = \nabla \cdot \vec{u} \quad (3.7)$$

As demonstrated by many textbooks (e.g. Jaeger et al., 2007; Love, 1944),  $\nabla \cdot \vec{u}$  is an invariant, meaning it remains unchanged when the coordinate system is transformed. Furthermore, it can be physically interpreted as the fractional change in the volume of the infinitesimal material particle,  $\delta(dV)/V$ , which is why it is also known as the *volumetric strain*.

Consequently, the strain tensor also provides information about changes in density. Assuming that the mass of the material particle doesn't change, the change in the local density,  $\rho_0$ , is, as proved by Lautrup (2011):

$$\delta\rho = -\rho_0 \nabla \cdot \vec{u} \quad (3.8)$$

As expressed in equation (3.8), various other properties or identities suggest the strain tensor, but the ones discussed here are likely the most useful for our purpose. In fact, we can consider the strain field as a tensor field that plays a crucial role in the theory of elasticity. We still need to address its counterpart, the stress tensor, to have the complete set of tools to study the planet's response.

### 3.2 Stress tensor

Stresses are internal forces that act across any imaginary internal surface drawn across a point within a deformable body. In addition, it is a measure of the force that adjacent material particles exert upon one another; therefore, it is intimately connected to the notion of pressure. Actually, the stresses are also measured as force per unit of area, or in Pascal, Pa.

To determine the state of stress at a point inside a body, we need to specify the stress across every plane passing through that point (Love, 1944). At first, this may seem impossible, considering that an infinite number of planes can be drawn through a point inside the body. However, this is precisely why the *stress tensor* exists. Cauchy's stress hypothesis states that we need at least nine numbers to indicate the state of stress in a given point, which are exactly the components of the stress tensor (Lautrup, 2011).

To clarify this, imagine an infinitesimal section of a randomly oriented plane

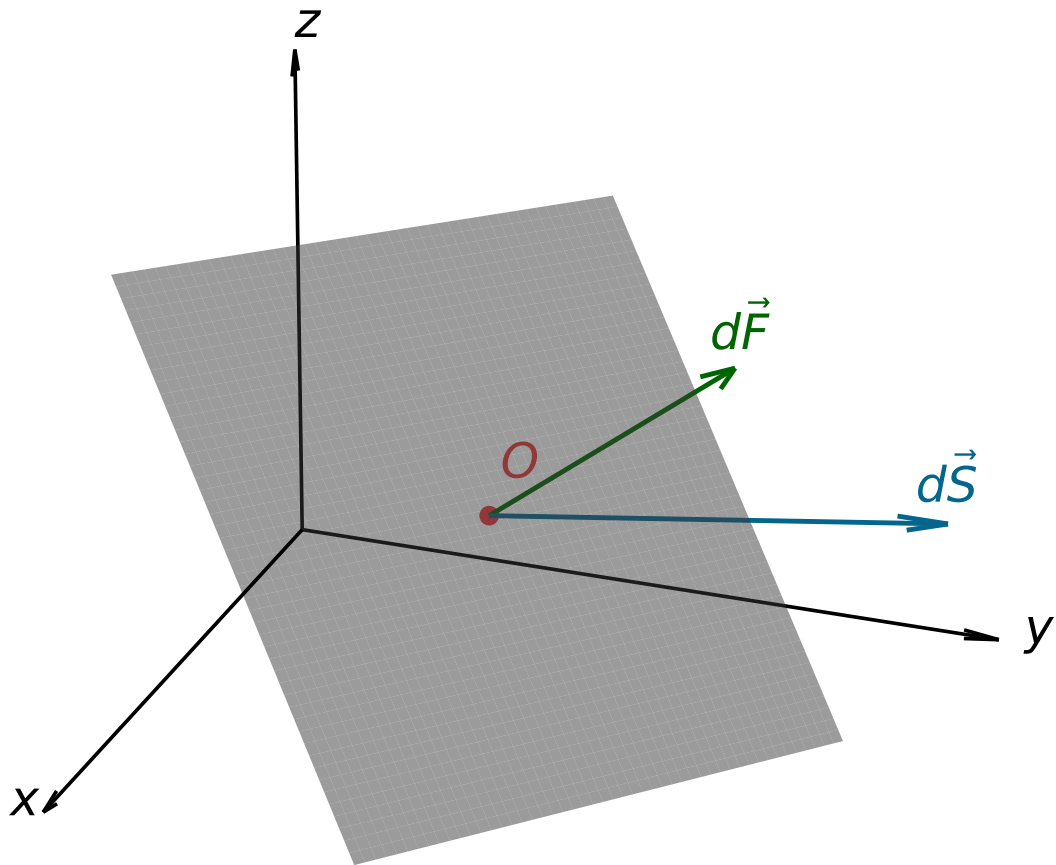


**Figure 3.2:** A force  $d\vec{F}$  acts on an imaginary plane passing through a point  $O$  inside a body. The plane is characterised by its normal vector  $d\vec{S}$ . We draw some Cartesian axes to suggest that both the force and the normal vector to the plane can be expressed in terms of their orthogonal components.

passing through a point  $O$  inside a body. The plane is defined by its normal vector  $d\vec{S}$  (as we see in Figure 3.2). A force  $d\vec{F}$  acts on this plane, exerted by the parts of the body above it, in the direction that  $d\vec{S}$  points. Therefore, the force per unit area at point  $O$  is given by  $d\vec{F}/d\vec{S}$ , with  $dS \rightarrow 0$ . Since both the force  $d\vec{F}$  and the normal vector  $d\vec{S}$  can be described by their components in an orthogonal coordinate system, we can write the components of the force acting on  $O$ , or the *traction in the direction of an specific axis*, for instance in the  $x$ -axis, as:

$$dF_x = \sigma_{xx} dS_x + \sigma_{xy} dS_y + \sigma_{xz} dS_z \quad (3.9)$$

In this equation, we have introduced the components of the *stress tensor*,  $\sigma_{ij}$ , with  $i, j = x, y, z$ , and the other components are expressed similarly. In  $\sigma_{ij}$ , the first subscript indicates the direction of the force, while the second subscript denotes the normal direction to the surface on which the force acts. Therefore, each component of the stress tensor can be defined as:

$$\sigma_{ij} = \frac{dF_i}{dS_j} \quad (3.10)$$

In a matrix notation, the stress tensor can also be written as:

$$\sigma_{ij} = \begin{pmatrix} \sigma_{xx} & \sigma_{xy} & \sigma_{xz} \\ \sigma_{yx} & \sigma_{yy} & \sigma_{yz} \\ \sigma_{zx} & \sigma_{zy} & \sigma_{zz} \end{pmatrix} \quad (3.11)$$

These components are the nine numbers referred to by Cauchy's stress hypothesis (the same as shown in Figure 3.3). However, the nine components can be reduced to six independent components, thanks to the equilibrium conditions imposed on  $\sigma$ . For instance, this tensor should fulfil the condition:

$$\sigma_{ij} = \sigma_{ji} \quad (3.12)$$

If we don't impose the condition (3.12), we can have torques on the material particles inside the solid bodies. Although this may be possible for some materials, it is common to enforce this symmetry on the stress tensor. Hence, the six independent components of the stress tensor are  $\sigma_{xx}$ ,  $\sigma_{yy}$ ,  $\sigma_{zz}$ ,  $\sigma_{xy}$ ,  $\sigma_{xz}$ , and  $\sigma_{yz}$ .

Using equation (3.9), and the components  $dS_j$  of the normal vector, we can also express the force, or the *traction on any surface  $dS$  across  $O$*  as:

$$\begin{aligned} d\vec{F}^{(S)} &= \sum_j (\sigma_{xj} dS_j, \sigma_{yj} dS_j, \sigma_{zj} dS_j) \\ &= (d\vec{F}_x, d\vec{F}_y, d\vec{F}_z) \\ &= \boldsymbol{\sigma} \cdot d\vec{S} \end{aligned} \quad (3.13)$$

Equation (3.13) implies, for instance, that if the  $d\vec{S}$  points in the direction of the  $x$ -axis, the traction on the plane perpendicular to that axis is:

$$d\vec{F}^{(S)} = (\sigma_{xx}, \sigma_{yx}, \sigma_{zx}) dS_x \quad (3.14)$$

The components of the form  $\sigma_{ii}$ , i.e., the diagonal entries, are known as *normal stresses*, because they point in the normal directions of the planes on which they act, as shown in Figure 3.3. Meanwhile, the components of the form  $\sigma_{ij}$  with  $i \neq j$ , i.e. the off-diagonal ones, are known as *shear stresses* because they are tangential to the planes on which they act. We didn't mention it before, but the same adjectives apply to the components of the strain tensor.

One of the simplest forms of the stress tensor arises in hydrostatic equilibrium. Since the pressure is the same in all directions, the diagonal entries have the same values, and at rest the fluids can't sustain shear stresses. Then, the stress

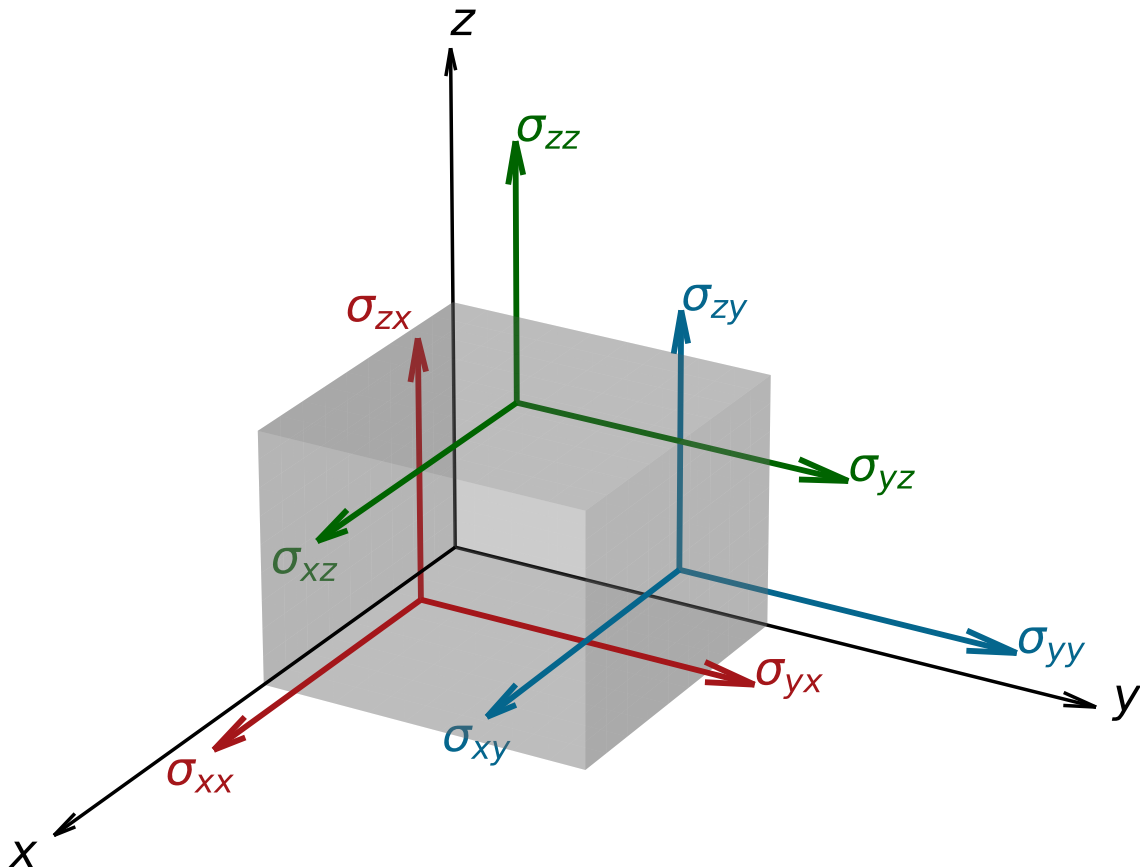


**Figure 3.3:** Visualisation of the nine components of the stress tensor on a material particle of volume  $dV$ . Note that, following our convention, the first index in  $\sigma_{ij}$  indicates the direction of the stress, while the second index indicates the plane on which the stress acts.

tensor has the form:

$$\sigma_{ij} = \begin{pmatrix} -p & 0 & 0 \\ 0 & -p & 0 \\ 0 & 0 & -p \end{pmatrix} = -p\delta_{ij} \quad (3.15)$$

From this form, we observe that the pressure is the average of the diagonal entries, and this is no coincidence. In general, the pressure can be defined as:

$$\sigma_{ij} = -\frac{1}{3}(\sigma_{xx} + \sigma_{yy} + \sigma_{zz}) = -\frac{1}{3}\text{tr}(\boldsymbol{\sigma}) \quad (3.16)$$

Again, more can be said about the stresses, including some interesting mathematical properties, but entire sections in specialised books are dedicated to this. For now, since we understand how to describe the forces acting on the surfaces of a body, our interest will be to write an equation of state and a relation between strain and stress.

### 3.3 Equation of motion

Consider an infinitesimal material particle, similar to the parallelepiped in the Figure 3.3. If the particle density is  $\rho$ , then the specific body force is  $\vec{f}$ , or  $\rho\vec{g}$  if we want to suggest that the gravity is the only body force<sup>1</sup>. From equation (3.13), we understand that the contact forces on the particle are  $\boldsymbol{\sigma} \cdot d\vec{S}$ . Consequently, the total force is the sum of the body force over the entire volume of the particle and the contact forces on each face:

$$\mathbf{F} = \int_V \rho\vec{g}dV + \oint_S \boldsymbol{\sigma} \cdot d\vec{S} = \int_V \rho\vec{g}dV + \int_V (\nabla \cdot \boldsymbol{\sigma}^T)dV \quad (3.17)$$

On the right side of equation (3.17), we employed the *Gauss's divergence theorem* to transform the surface integral into a volume integral. Furthermore, since (3.17) must hold for any volume, we can define an *effective density force* as:

$$\vec{f}^* = \rho\vec{g} + \nabla \cdot \boldsymbol{\sigma}^T \quad (3.18)$$

To obtain the total force, which should be consistent with *Newton's second law of motion*, we need to integrate each component of  $\vec{f}^*$  over the entire volume of the material particle. Therefore, this effective force should be equal to the body's specific inertia, which is connected to the second derivative of displacement:

---

<sup>1</sup>With "specific" we mean per unit volume.

$$\rho \left( \partial^2 \vec{u} / \partial t^2 \right) = \rho \vec{g} + \nabla \cdot \boldsymbol{\sigma}^T \quad (3.19)$$

Or in index notation:

$$\rho \left( \partial^2 u_i / \partial t^2 \right) = \rho g_i + \partial_j \sigma_{ij} \quad (3.20)$$

Equation (3.19) represents our general equation of motion, which naturally depends on the nature of the body forces and the form of the stress tensor. For instance, in cases of mechanical equilibrium, the right side of this equation should be zero. Also, regarding hydrostatic equilibrium, where any self-gravitating sphere, such as a planet, might be initially considered, it is understood that  $\vec{f}^* = 0$  and  $\sigma_{ij} = -\rho \delta_{ij}$  (as per equation (3.15)). Subsequently, in hydrostatic equilibrium, equation (3.19) becomes:

$$\nabla p = \rho \vec{g} \quad (3.21)$$

This is a well-known and useful equation; however, it is not suitable for analysing the planetary response, as we are specifically perturbing the planet's equilibrium state. According to Takeuchi & Saito (1972), certain properties of the undeformed hydrostatic equilibrium state are necessary to examine the perturbations caused by tides. Moving forward, it is important to distinguish between variables in hydrostatic equilibrium and those after deformation. For example,  $\rho_0$  and  $\vec{g}_0$  represent, respectively, the density and gravitational acceleration of Earth in hydrostatic equilibrium. Conversely,  $\rho$  and  $\vec{g}'$  denote the density after deformation and the gravitational acceleration induced by deformation. Additionally, we will refer to the positions in the equilibrium state as  $\vec{r} - \vec{u}$ , while reserving  $\vec{r}$  for the position in the deformed state<sup>2</sup>.

Fortunately, in previous sections, we introduced some mathematical identities that we will now use to analyse these quantities. For example, from equation (3.8), we know that the density after deformation at  $\vec{r}$  is the density at the undeformed state plus the change in density due to deformation:

$$\begin{aligned} \rho(\vec{r}) &= \rho_0(\vec{r} - \vec{u}) + \delta\rho = \rho_0(\vec{r} - \vec{u}) - \rho_0(\vec{r}) \nabla \cdot \vec{u} \\ &\approx [\rho_0(\vec{r}) - \vec{u} \cdot \nabla \rho_0] - [\nabla \cdot (\rho_0 \vec{u}) - \vec{u} \cdot \nabla \rho_0] \\ &\approx \rho_0(\vec{r}) - \nabla \cdot (\rho_0 \vec{u}) \end{aligned} \quad (3.22)$$

In the second line, we performed a first-order Taylor expansion of the term  $\rho_0(\vec{r} - \vec{u})$  and rewrote  $\rho_0 \nabla \cdot \vec{u}$  using the chain rule. Additionally, we can now

---

<sup>2</sup>This is a change in the notation that we used in section 3.1,  $\vec{X}$  and  $\vec{x}$ , but it is convenient to note that we are now moving to a spherically symmetric case, where some properties depend only on  $\vec{r}$ , and aligning with Takeuchi & Saito (1972).

calculate the stress tensor at the point  $\vec{r}$  in the deformed state. This stress tensor should consist of the initial stresses at the previous location  $\vec{r} - \vec{u}$ , which we can derive from equation (3.15), along with the additional stresses at  $\vec{r}$ , denoted by  $\sigma'_{ij}$  (Takeuchi & Saito, 1972):

$$\sigma_{ij} = -p_0(\vec{r} - \vec{u})\delta_{ij} + \sigma'_{ij}(\vec{r}) \quad (3.23)$$

From this equation, we see that all shear stresses in the deformed state arise from the additional stress; as previously mentioned, in hydrostatic equilibrium, shear stresses are absent. For normal stresses, there is also a pressure contribution. Performing a first-order Taylor expansion and using (3.21), we can derive an expression for this pressure:

$$p_0(\vec{r} - \vec{u}) \approx p_0(\vec{r}) - \vec{u} \cdot \nabla p_0 = p_0(\vec{r}) - \rho_0 \vec{g}_0 \cdot \vec{u} \quad (3.24)$$

Then, in spherical coordinates, the explicit components of the stress tensor are:

$$\begin{aligned} \sigma_{rr} &= -p_0(\vec{r}) + \rho_0 \vec{g}_0 \cdot \vec{u} + \sigma'_{rr} \\ \sigma_{\theta\theta} &= -p_0(\vec{r}) + \rho_0 \vec{g}_0 \cdot \vec{u} + \sigma'_{\theta\theta} \\ \sigma_{\phi\phi} &= -p_0(\vec{r}) + \rho_0 \vec{g}_0 \cdot \vec{u} + \sigma'_{\phi\phi} \\ \sigma_{r\phi} &= \sigma'_{r\phi}, \quad \sigma_{\theta r} = \sigma'_{\theta r}, \quad \sigma_{\theta\phi} = \sigma'_{\theta\phi} \end{aligned} \quad (3.25)$$

Or in a more compact notation:

$$\boldsymbol{\sigma} = (-p_0(\vec{r}) + \rho_0 \vec{g}_0 \cdot \vec{u}) \mathbf{I} + \boldsymbol{\sigma}' \quad (3.26)$$

Where  $\mathbf{I}$  is the identity matrix and  $\boldsymbol{\sigma}'$  is the matrix of the additional stresses. With (3.26), we have an expression for the stress tensor, but we still cannot substitute it into the general equation of motion before addressing the body forces, as they are now more complex. The total body forces in the perturbed situation include the *gravitational force*,  $\vec{g}_0$ , the *gravitational perturbation induced by deformation*,  $\vec{g}'$ , since deformation produces a change in density  $\delta\rho$ , and the *external body forces*  $\vec{g}_{ext}$  (Takeuchi & Saito, 1972). You probably already noticed that, strictly speaking, we expressed these forces in terms of accelerations, so that the specific forces are the density times the accelerations.

The gravitational perturbation induced by deformation can be expressed as the gradient of an additional potential  $\psi'$ , and in tidal problems, the external body force is derived directly from the TGP<sup>3</sup>:

---

<sup>3</sup>This potential corresponds to the one previously designated as  $V_{tid}$  in the preceding chapter.

$$\vec{g}' = \nabla\psi' \quad (3.27)$$

$$\vec{g}_{ext} = \nabla\psi_{TGP} \quad (3.28)$$

The TGP is harmonic, so it satisfies *Laplace's equation*, but the additional induced potential should satisfy *Poisson's equation* with the extra density that appears in equation (3.22) after the displacement:

$$\nabla^2\psi' = 4\pi G \nabla \cdot (\rho_0 \vec{u}) \quad (3.29)$$

Therefore, the total body force at  $\vec{r}$  is given by:

$$\begin{aligned} \vec{f}(\vec{r}) &= \rho(\vec{r}) [\vec{g}_0 + \vec{g}' + \vec{g}_{ext}] \\ &= [\rho_0 - \nabla \cdot (\rho_0 \vec{u})] [\vec{g}_0 + \nabla\psi' + \nabla\psi_{TGP}] \\ &\approx \rho_0 \vec{g}_0 + \rho_0 \nabla\psi' + \rho_0 \nabla\psi_{TGP} - \vec{g}_0 \nabla \cdot (\rho_0 \vec{u}) \end{aligned} \quad (3.30)$$

In the last line, we omitted some higher-order terms, as the additional density times the additional forces are very small compared with the undeformed density times the additional forces. Substituting the results of equations (3.26) and (3.30) into equation (3.19) yields the equation of motion for a self-gravitating sphere:

$$\rho_0 \frac{\partial^2 \vec{u}}{\partial t^2} = \nabla \cdot \boldsymbol{\sigma}'^T + \rho_0 \nabla\psi_{TGP} + \rho_0 \nabla\psi' - \vec{g}_0 \nabla \cdot (\rho_0 \vec{u}) + \nabla(\rho_0 \vec{g}_0 \cdot \vec{u}) \quad (3.31)$$

Equation (3.31) represents the equation of motion used to analyse the planet's response to tidal forces. Along with equation (3.29), these form the fundamental equations governing Earth's oscillations, as stated by Takeuchi & Saito (1972)<sup>4</sup>. Other forms of equation (3.31) are found in the literature, for instance in Xu & Sun (2003), but with some mathematical arrangements we can prove that they are equivalent.

Finally, to conclude this chapter, we review the fundamental relationship between stress and strain, which will be very helpful in deriving a solution to the equation (3.31).

## 3.4 Stress-strain relation

When physicists think of elasticity, a spring is probably one of the first objects that come to mind. The ability of springs to return to their original shape is what makes them elastic. Generally, this property defines the elastic behaviour of any

<sup>4</sup>Actually, Takeuchi & Saito (1972) say that these are the fundamental equations of free oscillations of the Earth. Still, we will see in chapter 4 that they are equivalent in principle, and the difference arises when we force certain boundary conditions.

object. However, this is an “ideal” behaviour because it assumes that objects can return exactly to their original state and that deformation is a reversible and adiabatic process. Even so, this approximation is quite reasonable because deformation can occur so quickly in many cases that almost no heat transfer takes place. Additionally, zero changes in temperature can be assumed. Under these assumptions, the energy stored due to deformation,  $W$ , must meet the condition:

$$\sigma_{ij} = \frac{\partial W}{\partial u_{ij}} \quad (3.32)$$

I strongly recommend reviewing the chapter on the elasticity of solid bodies in Love (1944) if you seek a detailed demonstration of the expression (3.32). Additionally, assuming elastic behaviour, the energy function should take a specific form. The *Generalised Hook’s law* establishes a proportionality between stress and strain, which can be expressed as each component of the stress at any point being a linear function of the strain components at that point (Lautrup, 2011; Love, 1944). To satisfy this law and condition (3.32),  $W$  should be a homogeneous and quadratic function of the strain components:

$$\begin{aligned} W = & \frac{1}{2}E_{xxxx}u_{xx}^2 + \frac{1}{2}E_{yyyy}u_{yy}^2 + \frac{1}{2}E_{zzzz}u_{zz}^2 + E_{xxxx}u_{xx}u_{xy} \\ & + E_{xxxx}u_{xx}u_{xz} + E_{yyyy}u_{yy}u_{xy} + E_{zzzz}u_{zz}u_{zx} + E_{yyyy}u_{yy}u_{yz} \quad (3.33) \\ & + E_{zzzy}u_{zz}u_{yz} + 2E_{xxyy}u_{xx}u_{yy} + 2E_{xxzz}u_{xx}u_{zz} + 2E_{yyzz}u_{yy}u_{zz} \\ & + 2E_{xxyz}u_{xx}u_{yz} + 2E_{yyxz}u_{yy}u_{xz} + 2E_{zzxy}u_{zz}u_{xy} \end{aligned}$$

Using this form, and differentiating with respect to  $u_{ij}$  (as suggested by equation (3.32)), we obtain an expression for the corresponding stress  $\sigma_{ij}$  as a linear combination of the strain components:

$$\sigma_{ij} = \sum_{k,l} E_{ijkl}u_{kl} \quad (3.34)$$

Where  $E_{ijkl}$  is the *elasticity tensor*. The various factors in equation (3.33) arise from the symmetry relations in the strain and stress tensors, which permit the interchange of certain indices. Additionally, in equation (3.33), we use  $E_{ijkl} = E_{lkij}$ , which stems from the relations that guarantee the existence of the function  $W$ , and  $E_{ijkl} = E_{iklj}$ , famously known as the *Cauchy’s relations*.

In equation (3.33), we have 15 different components of the elasticity tensor, which are proportionality coefficients between stress and strain that we do not know. Initially, we can state that, at each point on a body, these coefficients can take different values. However, there are some convenient situations, such as in the case of *completely isotropic materials*, where it is possible to reduce the coefficients to just two independent values at each point. In the case of completely

isotropic materials, the energy function can be expressed as follows (Lautrup, 2011; Love, 1944):

$$W = \frac{1}{2}(\lambda + 2\mu)(u_{xx} + u_{yy} + u_{zz})^2 + \frac{1}{2}\mu(e_{yz}^2 + e_{xz}^2 + e_{xy}^2 - 4e_{yy}e_{zz} - 4e_{xx}e_{zz} - 4e_{xx}e_{yy}) \quad (3.35)$$

Where  $\lambda$  and  $\mu$  are the *Lamé's coefficients*, material-dependent parameters. The form of the energy function in equation (3.35) also takes advantage of two mathematical invariants of the strain tensor under rotation, which is very convenient for writing the energy in an invariant form. Using equation (3.32), we can derive the components of the stress tensor from equation (3.35), yielding the following relation for shear stresses in isotropic materials:

$$\sigma_{ij} = \mu u_{ij} \quad \text{for } i \neq j \quad (3.36)$$

Thus,  $\mu$  is known as the *shear modulus*, as it always relates the shear components of stress and strain. In general, not just in the isotropic case, an elastic coefficient of any type is always defined as the ratio between the kind of stress required for a specific deformation and the resulting strain in that deformation (Love, 1944). For example, suppose we aim to apply a homogeneous compression to a material particle. In that case, we know that we must exert the same pressure on all faces, i.e.,  $\sigma_{ij} = -\delta_{ij}p$ , and that this is going to generate a volumetric strain given by  $\nabla \cdot \vec{u}$ , as we state in equation (3.7). Consequently, the *modulus of compression*, or *bulk modulus*, is given by the ratio of the needed pressure and the volumetric strain:

$$K = \frac{p}{\nabla \cdot \vec{u}} = \lambda + \frac{2}{3}\mu \quad (3.37)$$

Where the right side of the equation originates from deriving the equation (3.32), comparing it to the pressure, and isolating the elastic coefficients. Following the same reasoning, we can continue defining other well-known elastic moduli, such as the *Young's modulus*, which is:

$$E = \frac{\mu(3\lambda + 2\mu)}{\lambda + \mu} \quad (3.38)$$

For the moment, we are just going to say that these elastic coefficients are needed to calculate the planetary response to tides, and, luckily, they are related to the velocity of seismic waves in the planet's interior, which means they can be indirectly measured.

However, the completely isotropic case might not be the most relevant approximation in our subject. As explained by Takeuchi & Saito (1972), a planet

can resemble, at least in first approximation, a *transversely isotropic* material, more than a fully isotropic material, due to its layered structure. In this type of medium, the elastic coefficients exhibit symmetry in a plane or in two of the three orthogonal coordinates, while varying in the perpendicular direction to this plane. In this case, the energy function is expected to be (Takeuchi & Saito, 1972):

$$\begin{aligned} W = & \frac{1}{2}A(u_{xx}^2 + u_{yy}^2) + \frac{1}{2}Cu_{zz}^2 + F(u_{xx} + u_{yy})u_{zz} \\ & + \frac{1}{2}L(u_{yz}^2 + u_{xz}^2) + \frac{1}{2}N(u_{xy}^2 - 4u_{xx}u_{yy}) \end{aligned} \quad (3.39)$$

Where the medium is expected to change only along the  $z$ -axis. In spherical coordinates, with changes only in the radial direction, equation (3.39) becomes (Takeuchi & Saito, 1972):

$$\begin{aligned} W = & \frac{1}{2}A(u_{\theta\theta}^2 + u_{\phi\phi}^2) + \frac{1}{2}Cu_{rr}^2 + F(u_{\theta\theta} + u_{\phi\phi})u_{rr} \\ & + \frac{1}{2}L(u_{\phi r}^2 + u_{r\theta}^2) + \frac{1}{2}N(u_{\theta\phi}^2 - 4u_{\theta\theta}u_{\phi\phi}) \end{aligned} \quad (3.40)$$

Where the coefficients  $A$ ,  $C$ ,  $L$ , and  $N$  are related to the density,  $\rho$ , and velocity of seismic waves by:

$$\begin{aligned} v_{P_H} &= \sqrt{A/\rho} \quad \text{for horizontal P-waves} \\ v_{P_V} &= \sqrt{C/\rho} \quad \text{for vertical P-waves} \\ v_{S_H} &= \sqrt{N/\rho} \quad \text{for horizontal S-waves} \\ v_{S_V} &= \sqrt{L/\rho} \quad \text{for vertical S-waves} \end{aligned} \quad (3.41)$$

And the coefficient  $F$  can be approximated as:

$$F = \eta(A - 2L) \quad (3.42)$$

We can interpret  $\eta$  as a measure of the local anisotropy of the layered medium; for example, it equals 1 in an isotropic medium. Specifically, in an isotropic medium,  $A = C = \lambda + 2\nu$ ,  $N = L = \mu$  and  $F = \lambda$ . Note that all these elastic coefficients should be functions of the radius, since density and wave velocities vary with radius. That said, using relation (3.32), we can compute the stresses at each coordinate from the strain components:

$$\begin{aligned} \sigma_{rr} &= Cu_{rr} + F(u_{\theta\theta} + u_{\phi\phi}), \\ \sigma_{\theta\theta} &= Fu_{rr} + A(u_{\theta\theta} + u_{\phi\phi}) + 2Nu_{\phi\phi}, \\ \sigma_{\phi\phi} &= Fu_{rr} + A(u_{\phi\phi} + u_{\theta\theta}) + 2Nu_{\theta\theta}, \\ \sigma_{\theta\phi} &= Nu_{\theta\phi}, \quad \sigma_{\phi r} = Lu_{\phi r}, \quad \sigma_{r\theta} = Lu_{r\theta} \end{aligned} \quad (3.43)$$

Given the components outlined in (3.43), it is appropriate to revisit the equation of motion (3.31) to address the tidal response. Nevertheless, even with knowledge of a planet's material properties, such as the elastic coefficients at each radius, the solution still depends on the specific form of the displacement and the boundary conditions. It is also important to recognise that our equation of motion does not possess an analytical solution, even in the simplest scenario of a layered transversely isotropic sphere. Consequently, in section 5.2.1 we will examine an integration setup for solving the fundamental equations that govern the elastic response of planets to tidal forces, at least for Earth-like planets.

# 4 . Planetary response

In this chapter, we will calculate the elastic response of a planet to tidal forces. From the equation of state, we will derive the internal solutions, a set of coupled ODEs directly associated with the famous *Love numbers*, which contain all the necessary information to describe the additional stress, strain, and perturbing potential. As we will see, the numerical convergence of these ODEs is highly complicated due to their stiff nature, so different numerical setups have been proposed to solve the problem for Earth-like planets. We will discuss some approaches, and in the next chapter we will incorporate the successful setup into a Python package.

## 4.1 Spheroidal oscillations

To start, in the elastic regime we are concerned with how the planets vibrate, not with permanent deformation. As elucidated by Alterman et al. (1959) and Takeuchi & Saito (1972), a planet's oscillations can be classified into two categories: *torsional* and *spheroidal*. In purely torsional oscillations, the radial displacement and volumetric strain are zero, and thus this type of oscillation does not perturb the gravitational potential. Conversely, spheroidal oscillations are characterised by a vanishing radial component of the curl of the displacement about the vertical axis; however, they generate dilatation (non-zero volumetric strain) and perturb the gravitational potential. For this reason, spheroidal oscillations are responsible for the planet's deformation under a TGP. In this case, the components of the displacement can be expressed by (Alterman et al., 1959):

$$\begin{aligned} u_r &= y_1^n(r)V_n(\theta, \phi)e^{i\omega t}, \\ u_\theta &= y_3^n(r)\frac{\partial V_n(\theta, \phi)}{\partial \theta}e^{i\omega t}, \\ u_\phi &= y_3^n(r)\frac{1}{\sin \theta}\frac{\partial V_n(\theta, \phi)}{\partial \phi}e^{i\omega t} \end{aligned} \tag{4.1}$$

And the additional potential also has a similar mathematical form<sup>1</sup>:

---

<sup>1</sup>This includes the TGP at the location, plus the potential arising from the perturbation of the density.

$$\psi' = y_5^n(r) V_n(\theta, \phi) e^{i\omega t} \quad (4.2)$$

For equations (4.1) and (4.2),  $V_n(\theta, \phi)$  denote the surface spherical harmonics of degree  $n$ ,  $\omega$  is the angular frequency of the oscillation, and  $y_i^n(r)$  are radial functions to be determined. As we can see, the functions  $y_1^n(r)$  and  $y_3^n(r)$  are proportional to the radial and tangential components of the displacement, respectively, while  $y_5^n(r)$  is proportional to the perturbation of the gravitational potential.

Actually, solutions (4.1) and (4.2) were proposed for the free oscillations of planets. However, as we study in chapter 2, the TGP can be decomposed into sinusoidal signals of particular frequencies, with the spatial distribution described by spherical harmonics. That is, each component of the TGP at frequency  $\omega$  can resemble the term  $V_n(\theta, \phi) e^{i\omega t}$  in the spheroidal solutions, making solutions (4.1) and (4.2) also useful for describing the elastic response of planets to each component of the tidal signal.

## 4.2 Love numbers

In expressions (4.1) and (4.2), we can assume that  $V_n(\theta, \phi) e^{i\omega t}$  is dimensionless, so  $y_1^n(r)$  and  $y_3^n(r)$  have displacement units, while  $y_5^n(r)$  has potential units. Alternatively, we can assume that  $V_n(\theta, \phi) e^{i\omega t}$  is the actual potential, which implies that  $y_1^n(r)$  and  $y_3^n(r)$  should have units of inverse acceleration, and  $y_5^n(r)$  should be dimensionless, so that  $\vec{u}$  and  $\phi'$  have displacement and potential units, respectively. In this second approach, the spheroidal solutions can also be written in terms of the well-known *Love numbers*, the dimensionless coefficients  $h_n$ ,  $I_n$  and  $k_n$  defined by Love (1911) and Shida (1912), rather than  $y_i(r)$ :

$$\begin{aligned} u_r &= h_n \frac{V_n(\theta, \phi, r)}{g_0}, \\ u_\theta &= I_n \frac{1}{g_0} \frac{\partial V_n(\theta, \phi, r)}{\partial \theta}, \\ u_\phi &= I_n \frac{1}{g_0 \sin \theta} \frac{\partial V_n(\theta, \phi, r)}{\partial \phi}, \\ \psi' &= (k_n + 1) V_n(\theta, \phi, r) \end{aligned} \quad (4.3)$$

We have omitted the common factor  $e^{i\omega t}$ . Love numbers were originally proposed to describe the tidal response; consequently, they are the ideal analytical tool for the problem we are concerned with. From (4.3), we can readily state their relationship to the  $y_i^n(r)$  functions:

$$\begin{aligned} h_n &= y_1(r) g_0 \left( \frac{a_p}{r} \right)^n, \\ l_n &= y_3(r) g_0 \left( \frac{a_p}{r} \right)^n, \\ k_n &= y_5(r) \left( \frac{a_p}{r} \right)^n - 1 \end{aligned} \quad (4.4)$$

Note that the factor  $(a_p/r)^n$  in the relation between Love numbers and the functions  $y_i^n(r)$  allows us to cancel the radial dependence in the potential in equations (4.3), leading to the equations (4.1) and (4.2) for the potential on the surface.

### 4.3 Spheroidal strain, stress and potential

Using the spheroidal solutions for the displacement (equation (4.1)), we can first derive the strain from the definition given in equation (3.5). In spherical coordinates, the components of Cauchy's strain tensor are:

$$\begin{aligned} u_{rr} &= \frac{\partial u_r}{\partial r}, \quad u_{\theta\theta} = \frac{1}{r} \frac{\partial u_\theta}{\partial \theta} + \frac{u_r}{r}, \\ u_{\phi\phi} &= \frac{1}{r \sin \theta} \frac{\partial u_\phi}{\partial \phi} + \frac{u_r}{r} + \frac{u_\theta}{r} \cot \theta, \\ u_{r\theta} &= \frac{1}{2} \left( \frac{1}{r} \frac{\partial u_r}{\partial \theta} + \frac{\partial u_\theta}{\partial r} - \frac{u_\theta}{r} \right), \\ u_{r\phi} &= \frac{1}{2} \left( \frac{1}{r \sin \theta} \frac{\partial u_r}{\partial \phi} + \frac{\partial u_\phi}{\partial r} - \frac{u_\phi}{r} \right), \\ u_{\theta\phi} &= \frac{1}{2} \left( \frac{1}{r \sin \theta} \frac{\partial u_\theta}{\partial \phi} + \frac{1}{r} \frac{\partial u_\phi}{\partial \theta} - \frac{u_\phi}{r} \cot \theta \right) \end{aligned} \quad (4.5)$$

Substituting the spheroidal displacements into equations (4.5), we obtain:

$$\begin{aligned} u_{rr} &= \frac{dy_1}{dr} V_n, \quad u_{\theta\theta} = \frac{y_3}{r} \frac{\partial^2 V_n}{\partial \theta^2} + \frac{y_1}{r}, \\ u_{\phi\phi} &= \frac{y_3}{r \sin \theta} \left( \frac{1}{\sin \theta} \frac{\partial^2 V_n}{\partial \phi^2} + \cos \theta \frac{\partial V_n}{\partial \theta} \right) + \frac{y_1}{r} V_n, \\ u_{r\theta} &= \frac{1}{2} \left( \frac{(y_1 - y_3)}{r} + \frac{dy_3}{dr} \right) \frac{\partial V_n}{\partial \theta}, \\ u_{r\phi} &= \frac{1}{2} \left( \frac{(y_1 - y_3)}{r} + \frac{dy_3}{dr} \right) \frac{1}{\sin \theta} \frac{\partial V_n}{\partial \phi}, \\ u_{\theta\phi} &= \frac{y_3}{r \sin \theta} \left( \frac{\partial^2 V_n}{\partial \theta \partial \phi} - \cot \theta \frac{\partial V_n}{\partial \phi} \right) \end{aligned} \quad (4.6)$$

We omitted the subindex  $n$  from the  $y_i^n(r)$  functions for simplicity, but it is essential to remember that they depend on the potential's degree. Additionally, for simplicity, we will henceforth omit the  $e^{i\omega t}$  factor, as it does not influence the derivatives due to its dependence solely on time. Substituting the strain components from (4.6) into (3.43), we obtain the stress components:

$$\begin{aligned}
 \sigma_{rr} &= C \left( \frac{dy_1}{dr} V_n \right) + F \left( \frac{y_3}{r} \frac{\partial^2 V_n}{\partial \theta^2} + \frac{y_1}{r} V_n + \frac{y_3}{r \sin \theta} \left[ \frac{1}{\sin \theta} \frac{\partial^2 V_n}{\partial \phi^2} + \cos \theta \frac{\partial V_n}{\partial \theta} \right] + \frac{y_1}{r} V_n \right), \\
 &= \left[ C \frac{dy_1}{dr} + \frac{F}{r} (2y_1 - n(n+1)y_3) \right] V_n = y_2(r) V_n, \\
 \sigma_{\theta\theta} &= F \left( \frac{dy_1}{dr} V_n \right) + A \left( \frac{y_3}{r} \frac{\partial^2 V_n}{\partial \theta^2} + \frac{y_1}{r} V_n + \frac{y_3}{r \sin \theta} \left[ \frac{1}{\sin \theta} \frac{\partial^2 V_n}{\partial \phi^2} + \cos \theta \frac{\partial V_n}{\partial \theta} \right] + \frac{y_1}{r} V_n \right) \\
 &\quad - 2N \left( \frac{y_3}{r \sin \theta} \left[ \frac{1}{\sin \theta} \frac{\partial^2 V_n}{\partial \phi^2} + \cos \theta \frac{\partial V_n}{\partial \theta} \right] + \frac{y_1}{r} V_n \right) \\
 &= \left[ F \frac{dy_1}{dr} + \frac{A}{r} (2y_1 - n(n+1)y_3) - 2N \frac{y_1}{r} \right] V_n - 2N \frac{y_3}{r} \left( \frac{1}{\sin^2 \theta} \frac{\partial^2 V_n}{\partial \phi^2} + \cot \theta \frac{\partial V_n}{\partial \theta} \right), \\
 \sigma_{\phi\phi} &= F \left( \frac{dy_1}{dr} V_n \right) + A \left( \frac{y_3}{r} \frac{\partial^2 V_n}{\partial \theta^2} + \frac{y_1}{r} V_n + \frac{y_3}{r \sin \theta} \left[ \frac{1}{\sin \theta} \frac{\partial^2 V_n}{\partial \phi^2} + \cos \theta \frac{\partial V_n}{\partial \theta} \right] + \frac{y_1}{r} V_n \right) \\
 &\quad - 2N \left( \frac{y_3}{r} \frac{\partial^2 V_n}{\partial \theta^2} + \frac{y_1}{r} V_n \right) \\
 &= \left[ F \frac{dy_1}{dr} + \frac{A}{r} (2y_1 - n(n+1)y_3) - 2N \frac{y_1}{r} \right] V_n - 2N \frac{y_3}{r} \frac{\partial^2 V_n}{\partial \theta^2}, \\
 \sigma_{r\theta} &= \frac{L}{2} \left( \frac{(y_1 - y_3)}{r} + \frac{dy_3}{dr} \right) \frac{\partial V_n}{\partial \theta} = y_4(r) \frac{\partial V_n}{\partial \theta}, \\
 \sigma_{r\phi} &= \frac{L}{2} \left( \frac{(y_1 - y_3)}{r} + \frac{dy_3}{dr} \right) \frac{1}{\sin \theta} \frac{\partial V_n}{\partial \phi} = \frac{y_4(r)}{\sin \theta} \frac{\partial V_n}{\partial \phi}, \\
 \sigma_{\theta\phi} &= N \frac{y_3}{r} \left( \frac{\partial^2 V_n}{\partial \theta \partial \phi} - \cot \theta \frac{\partial V_n}{\partial \phi} \right) \frac{1}{\sin \theta}
 \end{aligned} \tag{4.7}$$

The calculated expressions resemble those given by Takeuchi & Saito (1972). Please note that we have now also defined the functions  $y_2^n(r)$  and  $y_4^n(r)$  as follows:

$$\begin{aligned}
 y_2^n(r) &= C \frac{dy_1}{dr} + \frac{F}{r} [2y_1 - n(n+1)y_3], \\
 y_4^n(r) &= \frac{L}{2} \left[ \frac{(y_1 - y_3)}{r} + \frac{dy_3}{dr} \right]
 \end{aligned} \tag{4.8}$$

To simplify the stress terms in (4.7), we also used a mathematical identity involving the angular Laplacian of spherical harmonics:

$$\nabla_{(\theta,\phi)}^2 V_n = \frac{\partial^2 V_n}{\partial \theta^2} + \frac{1}{\sin^2 \theta} \frac{\partial^2 V_n}{\partial \phi^2} + \cot \theta \frac{\partial V_n}{\partial \theta} = -n(n+1)V_n \quad (4.9)$$

The stress and strain should be continuous throughout the planetary body, i.e., the  $y_i^n(r)$  functions should be continuous. For this to also hold for the potential, the solutions should satisfy the condition (Takeuchi & Saito, 1972):

$$\nabla^2 \phi' - 4\pi G \nabla \cdot (\rho_0 \vec{u}) = \text{continuous} \quad (4.10)$$

Consequently, we consider it appropriate to define an additional function, as Alterman et al. (1959) did:

$$y_6(r) = \frac{dy_5}{dr} - 4\pi G \rho_0 y_1 \quad (4.11)$$

Using the provided definitions and the fundamental equations of motion, we now proceed to derive the ODEs that characterise our problem.

## 4.4 Differential equations for the elastic response

From the definitions of  $y_2$ ,  $y_4$ , and  $y_6$ , we can derive three of the six differential equations:

$$\begin{aligned} \frac{dy_1}{dr} &= \frac{1}{C} \left[ y_2 - \frac{F}{r} (2y_1 - n(n+1)y_3) \right] \\ \frac{dy_3}{dr} &= \frac{1}{r} (y_3 - y_1) + \frac{2}{L} y_4 \\ \frac{dy_5}{dr} &= y_6 + 4\pi G \rho_0 y_1 \end{aligned} \quad (4.12)$$

For the remaining equations, we use the equation of motion given by equation (3.31) and Poisson's equation in (3.29). The additional stresses and displacements in equation (3.31) are replaced by the equations (4.1) and (4.7), respectively<sup>2</sup>. From the radial component of the equation of motion, we obtain:

---

<sup>2</sup>Note that, in our case, the stresses at (4.7), denoted by  $\sigma_{ij}$ , are actually the additional stresses denoted in the equation of motion by  $\sigma'_{ij}$ . Do not confuse these two stresses, because in the context of the elastic planetary response,  $\sigma_{ij}$  are simply the stresses in the hydrostatic equilibrium state.

$$\begin{aligned} \frac{dy_2}{dr} = & -\omega^2 \rho_0 y_1 + \frac{2}{r} \left( F \frac{dy_1}{dr} - y_2 \right) + \frac{1}{r} \left( \frac{2(A-N)}{r} - \rho_0 g_0 \right) [2y_1 - n(n+1)y_3] \\ & + \frac{n(n+1)}{r} y_4 - \rho_0 \left( y_6 + 2 \frac{g_0}{r} y_1 \right) \end{aligned} \quad (4.13)$$

Also, by adding the polar and azimuthal components of the equation of motion, we get:

$$\begin{aligned} \frac{dy_4}{dr} = & -\omega^2 \rho_0 y_3 - \frac{F}{r} \frac{dy_1}{dr} - \frac{A}{r^2} [2y_1 - n(n+1)y_3] + \frac{2N}{r^2} (y_1 - y_3) \\ & - \frac{3}{r} y_4 - \frac{\rho_0}{r} (y_5 - g_0 y_1) \end{aligned} \quad (4.14)$$

We may have omitted some steps in the detailed derivation of equations (4.13) and (4.14), but there are no special tricks beyond expressing the spherical components of the divergence of the stress tensor. Finally, substituting the spheroidal solutions into equation (3.29) (Poisson's equation) yields:

$$\frac{dy_6}{dr} = -4\pi G \rho n(n+1) \frac{y_3}{r} + n(n+1) \frac{y_5}{r^2} - 2 \frac{y_6}{r} \quad (4.15)$$

As we suggested in section 3.4, the elastic coefficients can be determined from the seismic velocities in planetary interiors. We can also express  $A$ ,  $C$ ,  $L$ ,  $N$  and  $F$  as functions of the two Lamé coefficients, as shown in equation (3.35). Although planets more closely resemble a transversely isotropic case, this approximation is reasonable, on the basis that, when numerically integrating our ODEs, we can assume that, locally (at each radius), the planet's material is fully isotropic, and that variations in the elastic properties appear only when we jump to the next point or radius. In a completely isotropic case:

$$A = C = \lambda + 2\mu, \quad F = \lambda, \quad L = N = \mu \quad (4.16)$$

Furthermore, we can use these standard definitions to simplify our differential equations (Xu & Sun, 2003):

$$\beta = \lambda + 2\mu, \quad \gamma = \mu \frac{(3\lambda + 2\mu)}{\lambda + 2\mu}, \quad n_1 = n(n+1) \quad (4.17)$$

Substituting these definitions and the relations for the elastic coefficients into (??) yields:

$$\begin{aligned}
\frac{dy_1}{dr} &= -2\frac{\lambda}{\beta}\frac{y_1}{r} + \frac{y_2}{\beta} + n_1\frac{\lambda}{\beta}\frac{y_3}{r}, \\
\frac{dy_2}{dr} &= \left(-\rho\omega^2 r^2 - 4\rho gr + 4\gamma\right)\frac{y_1}{r^2} - 4\frac{\mu}{\beta}\frac{y_2}{r} + n_1(\rho gr - 2\gamma)\frac{y_3}{r^2} \\
&\quad + n_1\frac{y_4}{r} - \rho y_6, \\
\frac{dy_3}{dr} &= -\frac{y_1}{r} + \frac{y_3}{r} + 2\frac{y_4}{\mu}, \\
\frac{dy_4}{dr} &= (\rho gr - 2\gamma)\frac{y_1}{r^2} - \frac{\lambda}{\beta}\frac{y_2}{r} \\
&\quad + \left[-\rho\omega^2 r^2 + 2\frac{\mu}{\beta}\{(2n_1 - 1)\lambda + 2(n_1 - 1)\mu\}\right]\frac{y_3}{r^2} - 3\frac{y_4}{r} - \rho\frac{y_5}{r}, \\
\frac{dy_5}{dr} &= y_6 + 4\pi G\rho y_1, \\
\frac{dy_6}{dr} &= -4\pi G\rho n_1\frac{y_3}{r} + n_1\frac{y_5}{r^2} - 2\frac{y_6}{r}
\end{aligned} \tag{4.18}$$

Equations in (4.18) constitute the complete set of coupled ODEs required to study the planets' elastic response to tides<sup>3</sup>. Nevertheless, this set encounters difficulties when integrating through a liquid or fluid layer, where  $\mu = 0$ , because the third equation (for  $dy_3/dr$ ) diverges. Consequently, alternative sets of equations have been proposed in multiple references (Altermann et al., 1959; Longman, 1963; Chinnery, 1975; Saito, 1974). For instance, given that the tangential stress is zero in fluids ( $y_4 = 0$ ), Altermann et al. (1959) originally proposed the following set:

$$\begin{aligned}
\frac{dy_1}{dr} &= -2\frac{y_1}{r} + \frac{y_2}{\lambda} + n_1\frac{y_3}{r}, \\
\frac{dy_2}{dr} &= -\left(\rho\omega^2 + \frac{4\rho g}{r}\right)y_1 + n_1\rho g\frac{y_3}{r} - \rho y_6, \\
y_3 &= \frac{1}{r\omega^2}\left(g y_1 - \frac{y_2}{\rho} - y_5\right), \\
\frac{dy_5}{dr} &= 4\pi G\rho y_1 + y_6, \\
\frac{dy_6}{dr} &= -4\pi G\rho n_1\frac{y_3}{r} + n_1\frac{y_5}{r^2} - 2\frac{y_6}{r}.
\end{aligned} \tag{4.19}$$

However, it has already been recognised that this set of equations has some problems, especially the unphysically high and unstable tangential displacement

---

<sup>3</sup>Note that we are no longer using a subindex for the density and gravity. Still, you may remember that these values correspond to the undeformed situation in hydrostatic equilibrium.

in liquid layers for low-frequency tides, because  $\omega^2$  is dividing in the third equation of (4.19). For this reason, we won't follow this approach. Instead, we use the procedure of Amorim & Gudkova (2024). First, the authors called the functions  $y_i(r)$  in the outer region  $z_i(r)$ , so that, even though they have the same physical meaning, we can distinguish them. The authors avoid integrating all these functions and integrate only  $z_5$ , using a new function  $z_7$ , which is continuous throughout the region and defined as:

$$\begin{aligned} z_7 &= \frac{dz_5}{dr} + \frac{n+1}{r} z_5 - \frac{4\pi G\rho}{g} z_5 \\ &= z_6 + 4\pi G\rho z_1 + \left( \frac{n+1}{r} - \frac{4\pi G\rho}{g} \right) z_5 \end{aligned} \quad (4.20)$$

The differential equation for  $z_7$  is deduced in the same way as  $y_6$ , through Poisson's equation. Then, the set of equations in the liquid layer becomes:

$$\begin{aligned} \frac{dz_5}{dr} &= \left( \frac{4\pi G\rho}{g} - \frac{n+1}{r} \right) z_5 + z_7, \\ \frac{dz_7}{dr} &= \frac{2(n-1)}{r} \frac{4\pi G\rho}{g} z_5 + \left( \frac{n-1}{r} - \frac{4\pi G\rho}{g} \right) z_7 \end{aligned} \quad (4.21)$$

Boundary conditions are imposed on these equations through the following valid relations at the fluid core:

$$z_2 = \rho(gz_1 - z_5), \quad z_4 = 0 \quad (4.22)$$

In any case, both sets of equations (4.18) and (4.21) are stiff, and their numerical integration is highly complex. We will therefore implement a successful strategy from the literature to integrate them in the section 5.2 of the next chapter, taking into account the specific boundary conditions on the planets' surfaces and ensuring regularity at the planets' centres, to obtain a unique and physically meaningful solution.

## 4.5 Boundary conditions

At the surface of the planet, there are three boundary conditions that we should satisfy when integrating the equations of motion. The first two arise from the continuity of the stress tensor, i.e. the additional stresses. *Newton's Third Law of Motion* demands that, across a surface boundary, the two sides act on each other with equal and opposite forces, which can be written mathematically as (Lautrup, 2011):

$$\boldsymbol{\sigma}_1 \cdot \hat{\boldsymbol{n}} = \boldsymbol{\sigma}_2 \cdot \hat{\boldsymbol{n}} \quad \text{at} \quad r = a_p \quad (4.23)$$

Here,  $\hat{n}$  is a normal vector to the boundary surface, and  $\sigma_1$  and  $\sigma_2$  are the stress tensors on each side. For a free surface, the components of  $\sigma_2$  are zero; consequently, the components of  $\sigma_1$  should also be zero. As we saw in equations equation (4.7), the components of the stress are proportional to  $y_2$  and  $y_4$ ; therefore, the condition in equation (4.23) can be written as:

$$y_2(a_p) = y_4(a_p) = 0 \quad (4.24)$$

The third boundary condition arises from the continuity of the gravitational potential and its gradient at the planet's surface. Inside the planet, we know that the perturbing potential should take the form given by equation (4.2). Outside, the potential should take the form (Saito, 1974; Takeuchi & Saito, 1972):

$$\psi' = \left(\frac{r}{a}\right)^n V_n + D \left(\frac{a}{r}\right)^{n+1} V_n \quad \text{for } r \geq a_p \quad (4.25)$$

Where  $D$  is a constant determined by the boundary conditions. The first term in equation (4.25) arose from the TGP, and the second from the perturbation of the planet's density. Evaluating equations (4.2) and (4.25) at the surface ( $r = a_p$ ) and equating them, we get:

$$D = y_5(a_p) - 1 \quad (4.26)$$

By differentiating equations (4.2) and (4.25), using the definition of  $y_6$  in equation (4.11), evaluating at the surface, and equating the results, we obtain the boundary condition for the potential:

$$y_6(a_p) + \frac{n+1}{a_p} y_5(a_p) = \frac{2n+1}{a_p} \quad (4.27)$$

This condition should guarantee, after integrating the equations in (4.18), that the predicted perturbing potential at the surface matches the one measured by real geophysical measurements. Naturally, this will also depend on the quality of our model.

Furthermore, the boundary conditions may vary with the structure and composition of the chosen planetary interior model. For example, if a fluid layer exists within the planet, zero tangential stresses are expected on the boundary surfaces at the top and bottom of that layer, as fluids do not support shear stresses. This again yields  $y_4 = 0$  at those interfaces.

Some authors also impose discontinuity conditions on the pressure at certain interfaces to account for additional physical phenomena. For instance, additional pressure arising from centrifugal forces and differential rotation within specific layers would cause  $y_2$  to differ on either side of the layer interface (e.g., as implemented by Xu & Sun, 2003).

## 4.6 Solutions at the centre

One of the challenges in solving the ODEs of motion arises from the behaviour of the solutions at the planets' centres. Takeuchi & Saito (1972) state that "the most important point in the integration is that it should be carried out upward from below". This makes sense to us if our goal is to predict Love Numbers and surface perturbations, given the planet's structure and composition, but the authors originally said it because they were concerned about errors increasing when integrating in the downward direction.

We should therefore define the initial conditions for our numerical integration at the centre, and there are two commonly used approaches (Michel & Boy, 2021). In both cases, we recognise that it isn't possible to start the integration from  $r = 0$ , so we start from a small radius. There should be only three independent solutions because, even though the ODEs have six variables, three of them should be zero at the centre, namely the displacement and the perturbing potential, which means:

$$y_1 = y_3 = y_5 = 0 \quad \text{at} \quad r = 0 \quad (4.28)$$

With this in mind, the first option is to assume a homogeneous sphere of small radius,  $\delta r$ , centred on the origin, and to find the analytical solution at the surface of this sphere. This is possible because the ODEs in (4.18) have an analytical solution for the simplest case of a homogeneous, compressible, spherical planet, first derived by Love (1911). For anyone interested, Greff-Lefftz et al. (2005) reviewed analytical solutions that we will not cover here, as we will use the alternative approach.

The second approach is to define the small radius,  $\delta r$ , and, this time, expand the solutions  $y_i(r)$  in a power series about  $r = 0$ , as detailed by Crossley (1975). A Frobenius analysis yields the following solutions (Crossley, 1975):

$$\begin{aligned} y_1(r) &= Ar^{n-1} + A'r^{n+1} + \dots, \\ y_2(r) &= Br^{n-2} + B'r^n + \dots, \\ y_3(r) &= Cr^{n-1} + C'r^{n+1} + \dots, \\ y_4(r) &= Dr^{n-2} + D'r^n + \dots, \\ y_5(r) &= Er^n + E'r^{n+2} + \dots, \\ y_6(r) &= Fr^{n-1} + F'r^{n+1} + \dots \end{aligned} \quad (4.29)$$

Among the coefficients in (4.29), only three are independent and determined by the boundary conditions; the others are related to these by mathematical relations. Following Crossley (1975), Xu & Sun (2003) defined three independent solutions that can be integrated separately and then combined using the boundary conditions:

$$\begin{aligned}
y_{1,1} &= r^{n-1}, \quad y_{3,1} = 0, \quad y_{5,1} = 0, \quad (\text{first solution}) \\
y_{1,2} &= 0, \quad y_{3,2} = r^{n-1}, \quad y_{5,2} = 0, \quad (\text{second solution}) \\
y_{1,3} &= 0, \quad y_{3,3} = 0, \quad y_{5,3} = r^n, \quad (\text{third solution})
\end{aligned} \tag{4.30}$$

The remaining  $y_i$  functions in each independent solution can be easily derived using equations (4.8) and (4.11). As you can see, this proposal is consistent with the leading terms of the expansion in (4.29) and with the condition in (4.28). Note also that the second sub-index in the solutions (4.30) indicates the number of the independent solution, not the  $i$  in  $y_i$ . However, there is a more recent proposal in Amorim & Gudkova (2024) that uses the same tactic but includes higher-order terms in the expansion, making it more stable. They first propose the following solutions at the centre:

$$y_1 = cr^{n-1} + Cr^{n+1}, \quad y_3 = cr^{n-1} + Cr^{n+1}, \quad y_5 = Ar^n\Gamma \tag{4.31}$$

With  $\Gamma = 4\pi G\rho/3$ . This is again consistent with the expansion (4.29). As there should be only three independent coefficients, the constants  $c$  and  $b$  can be written as:

$$c = A \cdot Jn, \quad b = A \cdot J, \quad \text{with} \quad J = \frac{\Gamma}{n\Gamma - \omega^2} \tag{4.32}$$

Then, rewriting (4.31) with these constants yields three independent solutions defined by the constants  $A$ ,  $B$  and  $C$ . Again, using (4.8) and (4.11) to derive the remaining  $y_i$  functions, we found the set of initial conditions for each independent solution (Amorim & Gudkova, 2024):

$$\vec{y}^{A0}(r) = \begin{pmatrix} nJr \\ 2n(n-1)J\mu \\ Jr \\ 2(n-1)J\mu \\ \Gamma r^2 \\ n(1-3J)\Gamma r \end{pmatrix} r^{n-2}, \quad \vec{y}^{B0}(r) = \begin{pmatrix} 0 \\ -n(n+1)\lambda \\ r \\ n\mu \\ 0 \\ 0 \end{pmatrix} r^n,$$

$$\vec{y}^{C0}(r) = \begin{pmatrix} r \\ n\beta + 3\lambda + 2\mu \\ 0 \\ \mu \\ 0 \\ -3r\Gamma \end{pmatrix} r^n$$
(4.33)

Where the vectors  $\vec{y}$  contain the initial values for each  $y_i$  function. After integrating each of these solutions, the overall solution will be:

$$\vec{y}(r) = A\vec{y}^A(r) + B\vec{y}^B(r) + C\vec{y}^C(r) \quad (4.34)$$

Consequently, the constants  $A$ ,  $B$ , and  $C$  will be crucial for combining the individual solutions into the overall solution. However, we should not worry about their specific values now, as these will be determined at the final stage of the numerical integration to satisfy the boundary conditions. This approach is the one we will use to perform the numerical integration and address the problem of initial conditions in section 5.2 of the next chapter, as it yields more stable results.

Finally, we have all the basic theory required to compute the tidal potential and the elastic response to tides. In the next chapter, we will focus on those calculations and related planetary problems.

# 5 . Calculations

In this chapter, we explain how to perform key calculations: computing the TGP in the SS and integrating the ODE for a specific planet model. We also introduce TSPICE, a Python package for calculating the tidal potential and the elastic response of planets, which is important for various applications in geophysics and planetary science. After explaining the routines and integration process, we will discuss the package's features, its installation process, and provide examples of how to use it effectively.

## 5.1 Tidal Potential Calculations

In section 2.2, we derived mathematical expressions for calculating the TGP. We can use these expressions to compute it for any target body under the influence of other external bodies; however, for this purpose, we need specific physical data for each planetary body and relative ephemerides. Given a time,  $t$ , a position on the target body defined by its geographical coordinates,  $\theta$  and  $\phi$ , and its distance from the COM,  $a$ , what physical data do we need to calculate the TGP? From equation (2.17), we know that we need:

- The masses of each body, or the ratio between them,  $M_{ext}/M$ .
- The mean radius of the target body,  $a_p$ , or the radius that defines the reference acceleration  $g$ .
- The distance  $r$  between the two bodies at the time of the signal.
- The subpoint coordinates of the external body on the target body,  $\theta'$  and  $\phi'$ , at the time of the signal.

We also need to specify a maximum degree,  $n_{max}$ , because we must truncate the series at some point. Notice that we are using equation (2.17) because we want to report the potentials as heights above an equipotential surface, i.e.,  $V_{tid}/g$  rather than  $V_{tid}$ .

To obtain the physical data, we can use a query system such as *Astroquery* (Ginsburg et al., 2019), but this can be computationally expensive for

long calculations, for instance, over extended time intervals or across many locations. Instead, we propose using a well-known tool in celestial mechanics, *SPICE* from NASA’s Navigation and Ancillary Information Facility (NAIF) (Acton, 1996; Acton et al., 2018). SPICE is not just a toolkit but a complete system that utilises specific data files called *kernels*, alongside dedicated software originally released in Fortran and now supporting various programming languages. Community efforts have enabled the development of *SpiceyPy*, a Python wrapper for the toolkit that has expanded its accessibility (Annex et al., 2020). In appendix A we give a brief introduction to and explanation of the SPICE toolkit’s functions and kernels that we use here, in case anyone wants to replicate our calculations.

### 5.1.1 Calculation routine

Now, we summarise the calculation routine, emphasising the tools and methods used at each step. We may omit some “obvious” points because our focus is on the routine’s fundamentals rather than programming details; for example, we don’t explicitly cover installing Python packages or describe our code line by line. Nevertheless, the gaps are not deep, and we hope that, using this methodology, you can easily reproduce our calculations in other programming languages.

1. **Download and load the necessary kernels.** In the SPICE world, kernels are the heart of the system. They are files containing “low-level” ancillary data with physical or geometric information about various bodies, and can be used with the SPICE toolkit to determine higher-level information. These kernels come from different sources (spacecraft tracking over time, mission centres, science organisations, etc.) or can be created by us. For our purposes, we can access the official planetary kernels on [NASA’s NAIF website](#) and load them into our Python script using SPICE’s `furnsh` method. The loaded kernels should at least include information on the ephemerides of both the target and external bodies, their physical parameters (i.e., masses, shapes and sizes), the leap-seconds data, and the reference frame of the target body<sup>1</sup>.
2. **Obtain the planetary parameters from the kernels.** Once the kernels are loaded, we can use SPICE functions to obtain the necessary data. For the masses and radius, we can use the routine `bodvrd`. Given the name or ID of the bodies and the name of the property, e.g. ‘GM’ or ‘RADII’, this routine looks inside the planetary constants kernels for the required information. However, there are a few points to consider. First, SPICE kernels don’t store the masses but the gravitational parameter *GM*, which doesn’t affect our calculation, since the *G* factor doesn’t change the mass ratio. Also, the shape of the planetary bodies is assumed to be a triaxial ellipsoid, so we compute the mean radius using the three radii that SPICE returns. With the

<sup>1</sup>Once you are familiar with the SPICE designation, it is relatively easy to recognise what information each kernel contains. We expand on this in appendix A

masses and mean radius, we could calculate the reference gravitational acceleration using equation (2.12) if we wanted.

3. **Convert the time from Coordinated Universal Time (UTC) to Ephemeris Time (ET).** It is likely that, when we started our calculations, we defined the specific date or time window in the UTC frame, whereas the SPICE routines that compute ephemerides expect times in ET. Thus, we should convert the time to ET using the routine `utc2et`. If we are computing a time period, we should create an array with the appropriate interval from the initial and final times in ET.
4. **Calculate the distance between the bodies at each time step.** Using SPICE's `spkezr`, we obtain a state vector pointing from the external body to the target body at each time step, and the norm of these vectors gives the distance  $r$  between the bodies at each time. It is important to note that the output of `spkezr` depends on certain corrections (e.g. aberration or light-time travel between the bodies), but we will comment on this in appendix A, where we go through its inputs.
5. **Calculate the subpoint coordinates.** To obtain the subpoints, we use SPICE's `subpnt`, which takes as input important parameters, such as the body-fixed reference frame centred on the target body<sup>2</sup>. However, this routine returns rectangular coordinates, not geographical coordinates. We then use `recgeo`, with the information on the triaxial ellipsoid that characterises the target body obtained in step 2, to convert the rectangular coordinates into geographical coordinates of the subpoint.
6. **Calculate the potential series terms.** We now have the masses, radius, distances, and subpoint coordinates at each time, so we can compute each term in equation (2.17). For this, we need two main iterations: the first over the degree, from  $n = 2$  to  $n = n_{\max}$ , and a second for each degree over the orders, from  $m = -n$  to  $m = n$ . For each degree, we compute the coefficient  $K_n(a)/r(t)^{n+1}$  and the sum over the order of the product of the spherical harmonics for the observer location and the conjugate spherical harmonics for the subpoint coordinates,  $\bar{Y}_n^m(\theta', \phi') Y_n^m(\theta, \phi)$ . The result of the sum, multiplied by the coefficient, gives us the  $n$ -th term. It is important to note that, for the spherical harmonic calculations, we use SciPy routines (Virtanen et al., 2020), so we should verify that we provide all coordinates in radians. Also, remember that  $\theta$  is a colatitude in equation (2.17).
7. **Calculate the potential series terms.** Once we have computed the series terms, we can sum them to obtain the total signal. The result is the value of  $V_{\text{tid}}/g$  on the target body due to the specific external body. However, if there is more than one external body, e.g., we want the Earth tides due to

---

<sup>2</sup>This is why it is important to have previously loaded a frame kernel for the target body; otherwise, the routine `subpnt` won't work.

the Moon, Sun and planets, we should repeat the from step 1 to step 5 for each external body, and add all the terms to obtain the total  $V_{\text{tid}}/g$  on the target body due to the list of external bodies.

We test this routine with some interesting examples, starting with the Earth, where lunisolar tides have been extensively studied and where other software allows us to verify our results. We then calculate the tides on the Moon to compare its frequencies with those of the Earth's tides. Finally, we compute the TGP for Io, where the geological effects of tidal dissipation are of great interest to planetary scientists.

### 5.1.2 Tides on the Earth

We already showed the TGP signal on Earth due to the Moon, and the combined signal due to the Moon, Sun and planets, in Figure 2.4 and Figure 2.5, respectively, and briefly discussed them in section 2.4. However, to ensure that our routine, and hence the Python package we created to implement it, works correctly, we can use an independent tool to calculate the tidal signals. One of the most widely used software packages in the geophysics community is *ETERNA*, originally created by Wenzel (1996) and updated to *ETERNA-x* in more recent years by Schueller (2020). Nevertheless, there are a few important considerations to bear in mind.

*ETERNA-x* doesn't directly return the TGP, but instead computes derived signals such as the perturbing potential, tidal displacements (as in equation (4.3)), and strain components. To perform these calculations, the software uses TGP catalogues to reconstruct the signal from its harmonic components (a different approach from that implemented in TSPICE). It also includes catalogues of the Love numbers at different frequencies and for different models, so that when summing the harmonic components, each component is weighted by the corresponding Love number of the chosen model. As a result, we can't directly compare the magnitudes of our signal with those returned by *ETERNA-x*, but both signals should show the same frequencies in a Fourier analysis.

Figure 5.1 shows the TGP computed with TSPICE and the potential returned by *ETERNA-x* for a complete year at the same location. It is evident that both signals share the same patterns, but the *ETERNA-x* signal reaches higher values. In the lower panel of that figure, we zoom in on the first month and confirm that both signals appear to have approximately the same phase. This doesn't replace a proper Fourier analysis of both signals, so in Figure 5.2 we display the tidal spectrum of the *ETERNA-x* signal, which shows a strong resemblance to the one in Figure 2.6. In fact, both spectra show the same peaks, confirming that both signals are composed of the same frequencies.

It would also be interesting to use our routine to examine the global distribution of the TGP and its temporal evolution. So far, we have considered specific locations on Earth, but we can create a grid of latitudes and longitudes at the surface and then calculate the potential at each point. Figure 5.3 shows the global distribution of the TGP on Earth due to the Moon, Sun and planets over approximately a month. We chose five moments during the month, separated by

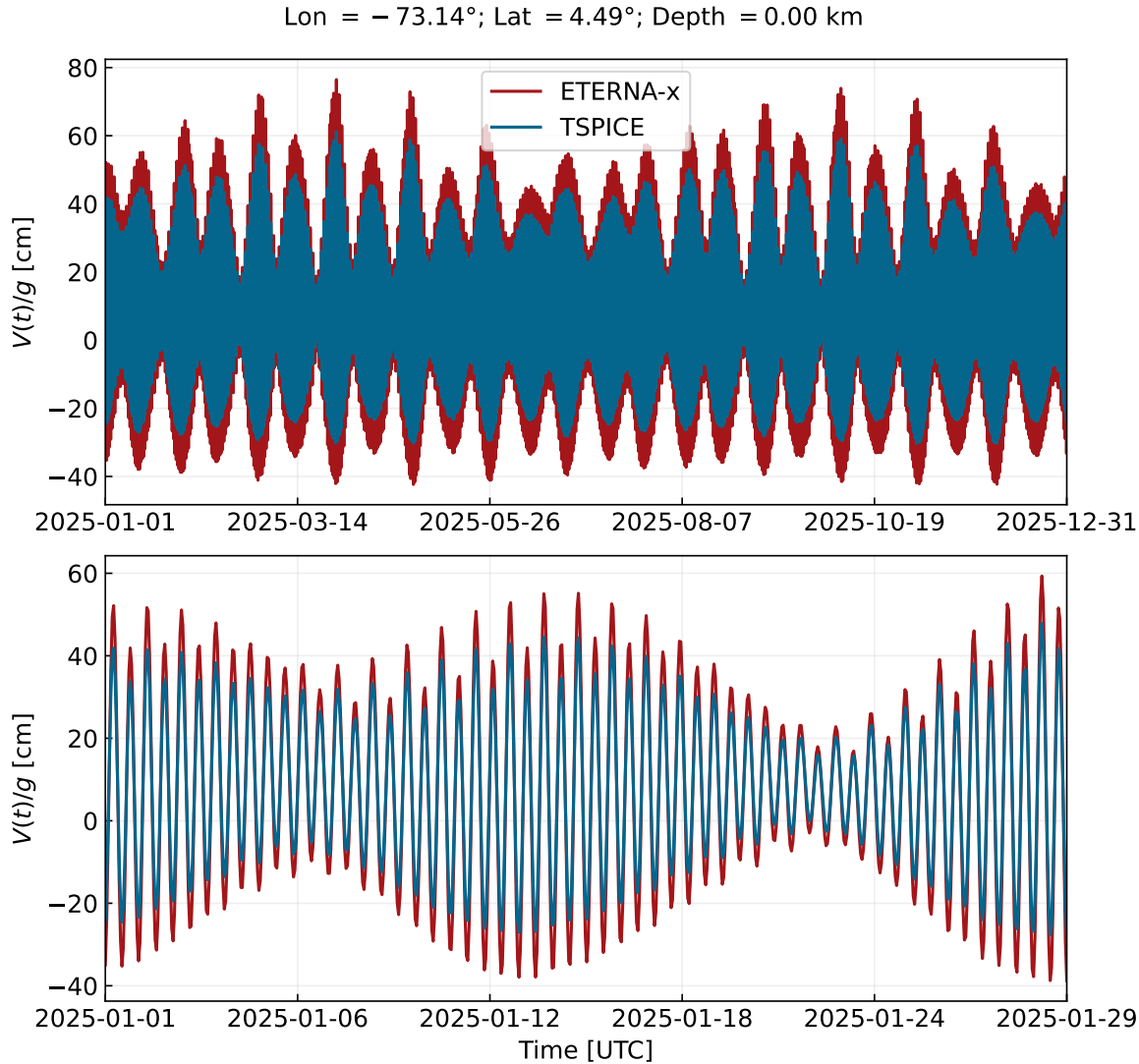


**Figure 5.1:** Tidal signals obtained with TSPICE and ETERNA-x. In the upper panel, we show the signals for a full year, and in the lower panel, we show the signals for the first month only. As expected, the TSPICE signal is lower than the one retrieved with ETERNA-x, which is scaled by the Love numbers at each frequency. Both signals were computed at one-hour intervals at the same location.

seven days, roughly corresponding to the time the Moon takes to go from one phase to the next. From that sequence, it is evident how the potential affects the well-known phenomenon of the *spring and neap tides*: we see an alternation between strong and moderate potential gradients every seven days.

### 5.1.3 Tides on the Moon

The Moon provides an excellent case for comparing the TGP. Computing the TGP on the Moon allows us to examine how the signal differs on the opposite side of the system. Figure 5.4 shows the tidal signal on the Moon at a surface location,

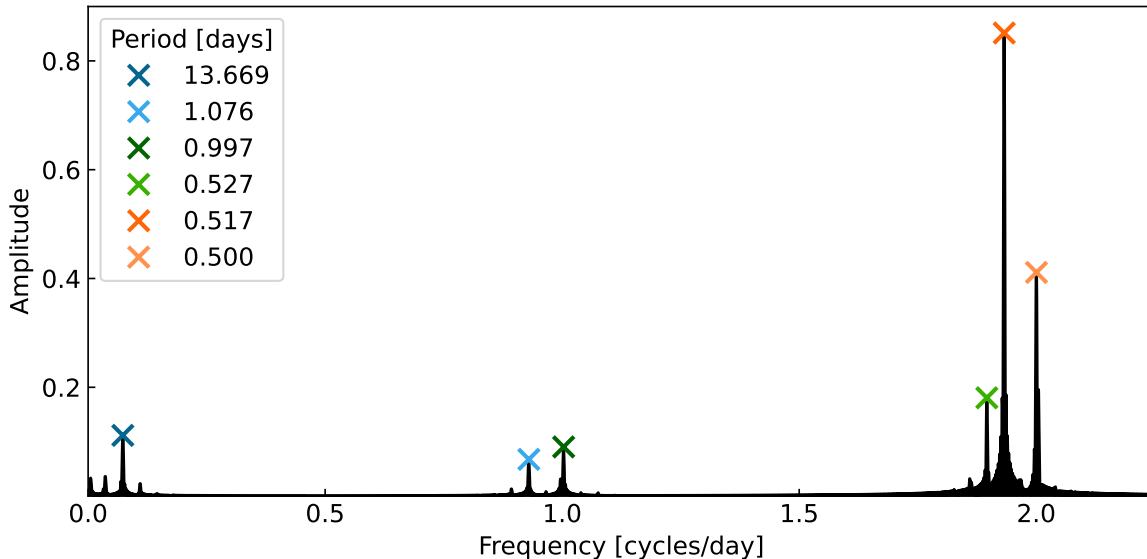


**Figure 5.2:** Spectrum of the tide-generating potential on Earth. The spectrum was computed from the ETERNA-x signal shown in Figure 5.1. We used LombScargle from Astropy to determine the frequencies and their corresponding amplitudes. The spectrum resembles the one we previously showed in Figure 2.6 for the TSPICE-computed signal.

due to the Earth, Sun, and planets over a complete year. The figure shows both the time-domain signal and its frequency spectrum. At first glance, the signal looks very different from that of the Earth. We quickly notice the absence of the diurnal and semidiurnal variations seen on Earth. This is also reflected in the tidal spectrum, which shows peaks at lower frequencies or longer periods only.

The principal tides on the Moon arise from the Earth-Moon orbital dynamics, with the stronger components occurring over the lunar month ( $\sim 27.9$  days). Nevertheless, the spectrum in Figure 5.4 also shows peaks at the fortnightly frequencies (around 14 days) and prominent peaks in the long-period band (the 214.7 days peak).

Furthermore, the magnitude of the tidal potential on the Moon is approximately one order of magnitude greater than that at Earth locations, due to Earth's stronger gravity (the potential is proportional to the mass of the external body in equation (2.7)). These observations, together with the fact that the Moon is also a rocky body that can be studied under the elastic regime, underscore the importance of considering the Moon's tidal potential and its responses in future studies.

#### 5.1.4 Tides on Io

Io represents perhaps the most extreme tidal environment in the SS. As one of Jupiter's Galilean moons, Io orbits at a distance of only approximately 422,000 km from Jupiter's centre, placing it well within the giant planet's dominant gravitational sphere of influence. Unlike Earth and the Moon, where we still consider the influence of the Sun and, to a lesser extent, other planets, Io is subjected to an

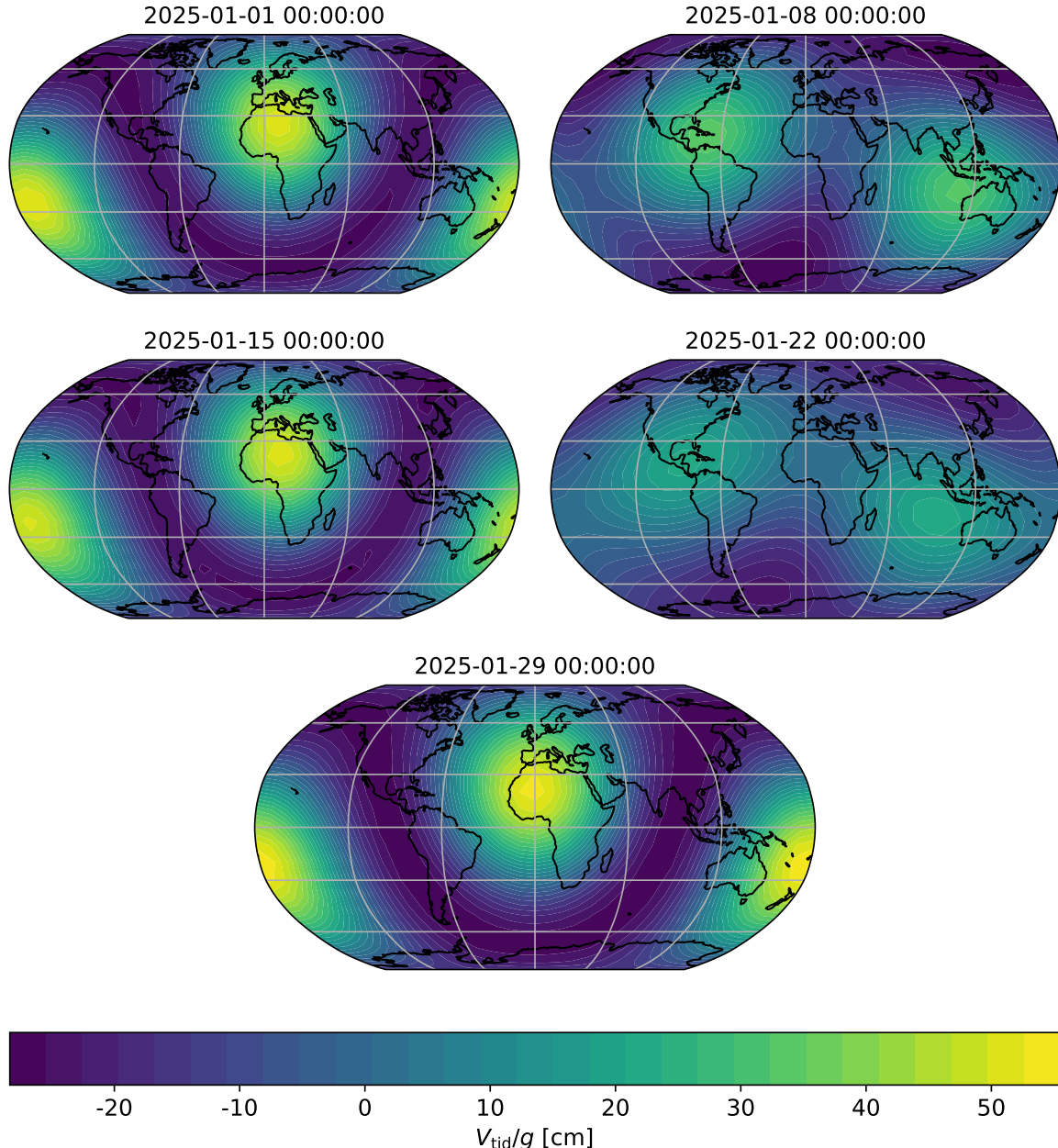


**Figure 5.3:** Global distribution on the Earth's surface of the tide-generating potential due to the Moon, Sun and planets over approximately a month, throughout January 2025. The contours show the potential values, expressed in centimetres relative to the reference equipotential surface, and the potential was computed up to  $n_{\max} = 6$ . The subplots in the figure are separated by seven days, allowing us to see the lunar phase cycle in sequence and revealing the characteristic pattern of spring and neap tides as the relative geometry of the Earth–Moon–Sun system evolves.

overwhelmingly strong tidal potential dominated by Jupiter's gravity. This extreme tidal forcing has profound consequences for Io's internal structure and geology.

The tidal potential environment on Io is characterised by enormous amplitude

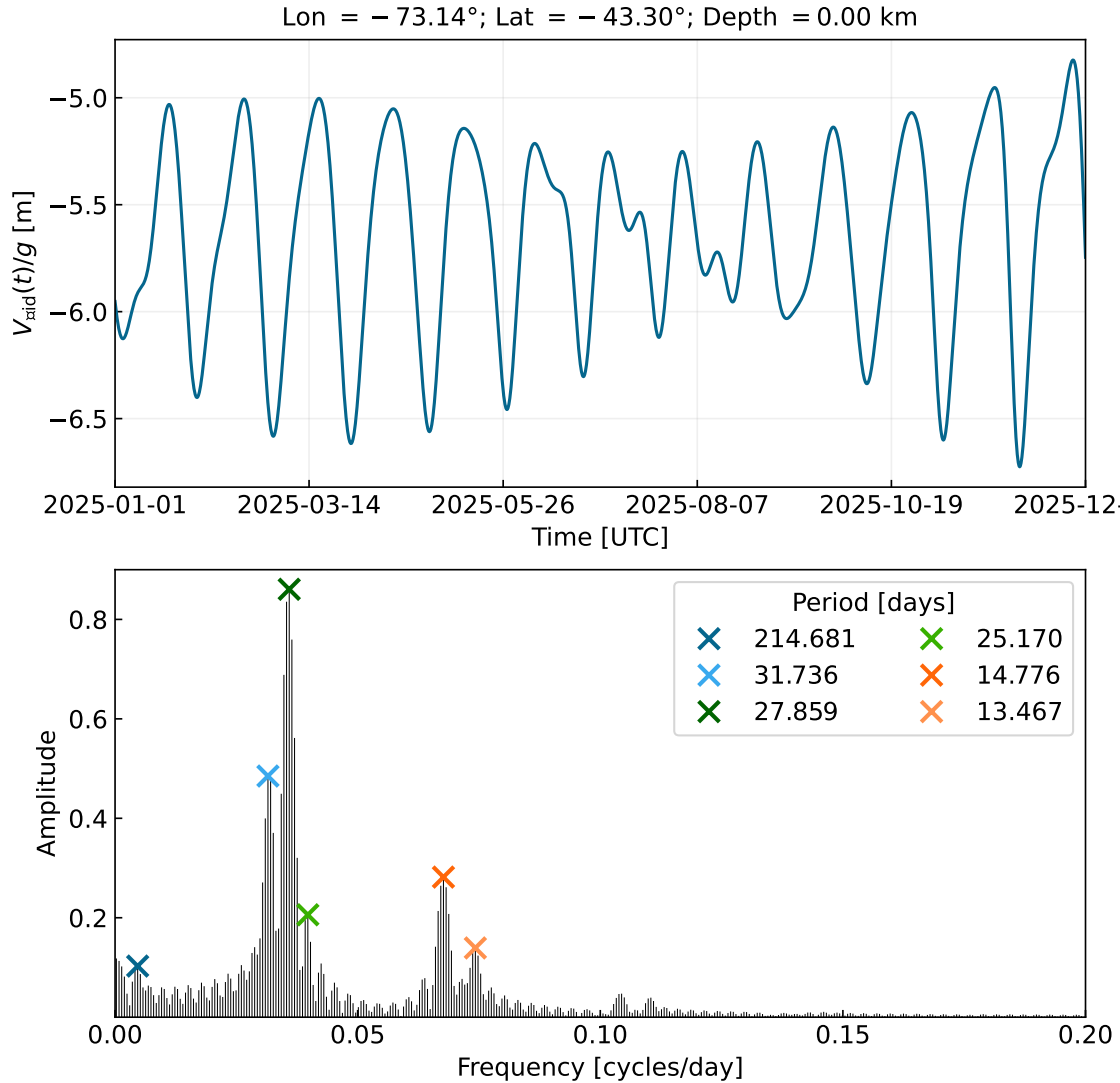


**Figure 5.4:** Tidal signals on the Moon computed with TSPICE. The upper panel shows the time-domain tide-generating potential at a selected location on the lunar surface over approximately one month, due to the combined gravitational influence of the Earth, Sun, and planets, computed up to  $n_{\max} = 6$ . The lower panel displays the frequency spectrum of the signal, revealing the dominant harmonic components. Note that the more prominent peaks are closer to the Moon's orbital period around the Earth.

variations driven almost entirely by Jupiter's gravitational influence. The magnitude of the TGP on Io is several orders of magnitude greater than that experienced by the Earth or Moon, owing to Jupiter's vast mass and Io's proximity (see equation (2.7)). Figure 5.5 shows this signal at the famous eruptive centre Loki on Io over a month. This intense potential could have significant consequences for Io's interior and deformation processes.

Figure 5.5 also shows the spectrum of this signal, confirming once again that the TGP on Io is dominated by Io's orbital period around Jupiter, approximately 1.77 days. The spectrum shows that the principal tidal component corresponds

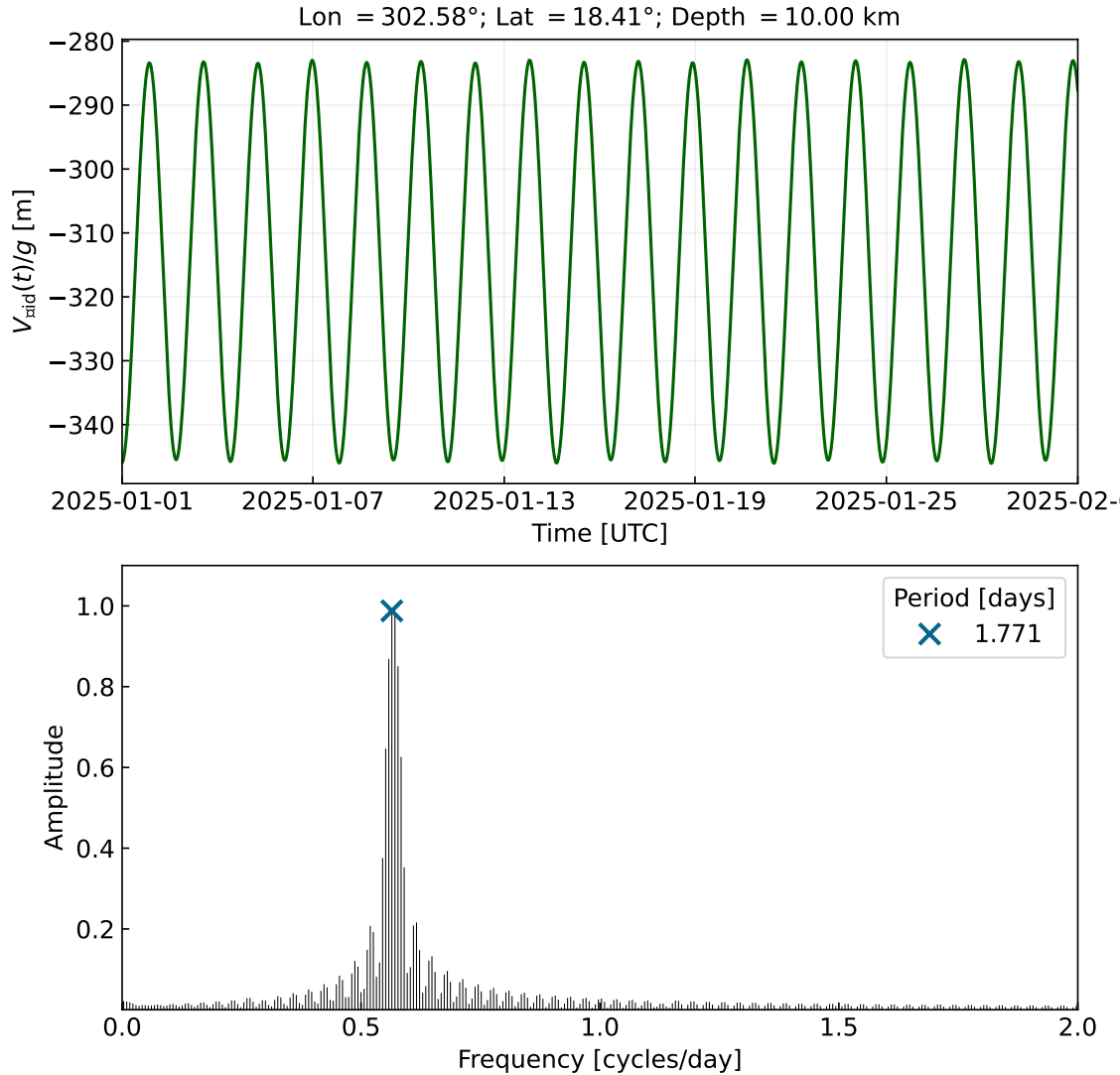


**Figure 5.5:** Tide-generating potential on Io, computed with TSPICE due to Jupiter. The upper panel shows the time-domain signal at a selected location on Io's surface (the eruptive centre Loki) over approximately one month, computed up to  $n_{\max} = 6$ . The lower panel displays the tidal spectrum, revealing the dominant harmonic components. The signal is dominated by Jupiter's potential at Io's orbital period around the planet, and hence the spectrum shows essentially the peak associated with that orbital motion (corresponding to  $\sim 1.77$  days) and its harmonics, with negligible contributions from the Sun, Saturn, or other moons in the system. The extreme amplitude of Io's tidal signal, which is orders of magnitude larger than Earth's or the Moon's, drives the intense tidal dissipation and associated volcanic activity that characterise this moon.

to the orbital frequency and its harmonics, with no meaningful contribution from longer-period components arising from the orbital periods of the Sun or other planetary bodies. Consequently, for Io, the tidal potential problem reduces, for all practical purposes, to a two-body problem of the Io-Jupiter system.

## 5.2 Love numbers Calculations

As shown in chapter 4, the planetary response to the TGP is described by the first-order coupled ODEs (4.18) for the functions  $y_i(r)$ . By determining these functions' values at the planetary surface, we can compute the Love numbers using equation (4.4). Consequently, these Love numbers are the essential parameters that characterise the planetary response and are commonly reported in the scientific literature. However, we now know that their values depend strongly on the planets' mass distribution and elastic properties, as well as on the frequency and degree of the tidal potential.

Therefore, before attempting to integrate the ODEs, a planetary model must be defined. These models should be in hydrostatic equilibrium and satisfy mass conservation. Depending on the model, the numerical integration strategy may vary. It is not the same to integrate a planet with a fluid layer at its centre as one with an intermediate fluid layer, or one that is completely solid. As we mentioned, equations (4.18) are singular when  $\mu = 0$ , so we may use an alternative system of equations, but the initial conditions may also differ.

Since the Earth's Love numbers are known from real geophysical measurements, we can first try to reproduce them using the PREM (Dziewonski & Anderson, 1981). In this model, the Earth has multiple discontinuities in its mass distribution, but the two most important are the ICB and the CMB, which separate the inner core from the outer core and the core from the mantle, respectively. For us, these two discontinuities also separate the integration over the fluid outer core from that over the rest of the planet. Figure 5.6 shows the profiles of the density, gravity and elastic parameters for the PREM, with a modification suggested by Amorim & Gudkova (2025) to the top layer of the Earth, where the ocean is replaced by a solid layer with  $\rho = 2178.9 \text{ kg/m}^3$ ,  $\mu = 266.6 \text{ kbar}$  and  $K = 520 \text{ kbar}$ . In the figure, you can also see the locations of the ICB and the CMB, and between them the outer core with zero shear modulus. So, essentially, we will have to worry about three integration regions: first, a solid layer for  $r \leq c$ , then a fluid layer in  $c < r \leq b$ , and finally, a solid region extending from  $r > b$  to the planet's radius  $a_p$ .

### 5.2.1 Integration setup

With this planetary profile, we can integrate the ODEs using any of the integration methods reported in the literature (Amorim & Gudkova, 2024; Xu & Sun, 2003; Michel & Boy, 2021). In this work, we follow the detailed proposal from Amorim & Gudkova (2024).

- 1. Define the integration parameters.** We need to define the principal integration parameters: the initial radius at the centre, the boundary radii, and the step size. Here, we should also define the degree,  $n$ , and the frequency,  $\omega$ , associated with the harmonic component of the tide.

The initial radius,  $r_0$ , is the radius at which we start the integration from the core and should be small enough to ensure that the power series expansion

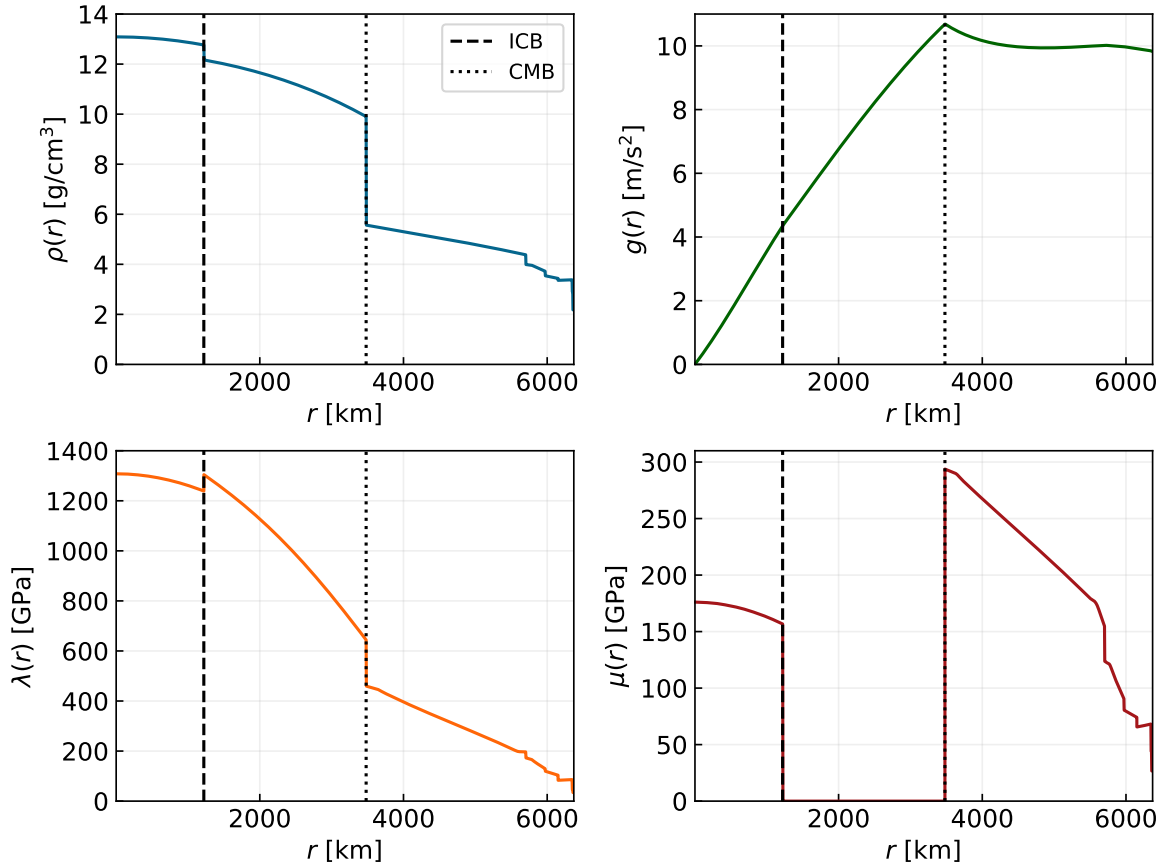


**Figure 5.6:** Planetary profiles from the PREM, modified as in (Amorim & Gudkova, 2025). The density (top left), gravitational acceleration (top right), shear modulus (bottom left), and elastic modulus (bottom right) are shown as functions of the planet's radius. Compared with the original Preliminary Reference Earth Model (PREM), the ocean layer is replaced by a solid layer with  $\rho = 2178.9 \text{ kg/m}^3$ ,  $\mu = 266.6 \text{ kbar}$ , and  $K = 520 \text{ kbar}$ . The Inner Core Boundary (ICB) (dashed line) at approximately 1220 km and the Core-Mantle Boundary (CMB) (dotted line) at approximately 3480 km are indicated. Note the zero shear modulus between the two lines, indicating fluid behaviour in the outer core.

for the initial conditions is valid. The boundaries are defined by the planetary model. The step size,  $\Delta r$ , should be small enough to ensure numerical stability and accuracy, but not so small that the computation becomes inefficient. Alternatively, we can specify a total number of steps, from which the step size is deduced. We can also define different step sizes or the number of steps per layer, if needed.

2. **Rescale the equations.** Integrating with values in SI units is inconvenient because of the large differences in magnitude among some physical parameters. To reduce the propagation of errors arising from these differences, we convert the physical values into a convenient dimensionless system where:

$$\begin{aligned} r &= \tilde{r}a_p, & m &= \tilde{m}M_p, & \rho &= \tilde{\rho}\rho_0, & g &= \tilde{g}g_0, \\ \mu &= \tilde{\mu}P_0, & \lambda &= \tilde{\lambda}P_0, & \omega &= \tilde{\omega}\omega_0 \end{aligned} \quad (5.1)$$

This allows us to write a new version of the equations (4.18) in terms of dimensionless quantities, with the gravitational constant  $G$  set to 1. The scale coefficients, such as  $\rho_0$ ,  $P$  and  $g_0$ , can also be expressed in terms of the body's key physical parameters and the constant  $G$ , as follows:

$$\rho_0 = \frac{M_p}{a_p^3}, \quad g_0 = \frac{GM_p}{a_p^2}, \quad P_0 = \frac{GM_p^2}{a_p^4}, \quad \omega_0 = \sqrt{\frac{GM_p}{a_p^3}} \quad (5.2)$$

3. **Interpolate the data from your planetary model.** Profiles as in Figure 5.6 should be interpolated as numerical functions that the integrator will receive. To ensure the best transition between layers and avoid numerical problems, I recommend interpolating within each layer rather than using a single interpolation over the entire planet. Of course, these numerical functions should depend on  $\tilde{r}$  and be dimensionless.
4. **Define the initial conditions at the centre.** We define the three independent initial solutions, given by equations (4.33), for the functions  $y_i(r)$  at  $r_0$ . These initial values should also be dimensionless, and since they depend on the degree  $n$  and the frequency  $\omega$ , they should be recalculated for each integration.
5. **Integrate the ODEs in the inner core.** We express the system in (4.18) as a function that the integrator can use. We then integrate the three independent solutions from  $r_0$  to  $c$  using a suitable numerical integrator for ODEs. In our case, we use *SciPy*'s `solve_ivp` with the BDF method (Virtanen et al., 2020) for these and the forthcoming integrations. Figure 5.7 shows the results of the integration for the PREM for each independent solution.
6. **Combine and define an initial solution for the outer core.** Before following the integration at the outer core, we combine the solutions as in equation (4.34) at  $r = c$ , where the boundary conditions and relations in (4.22) yield<sup>3</sup>:

---

<sup>3</sup>Note that we are not going to assume continuity of tangential displacements in the outer core.

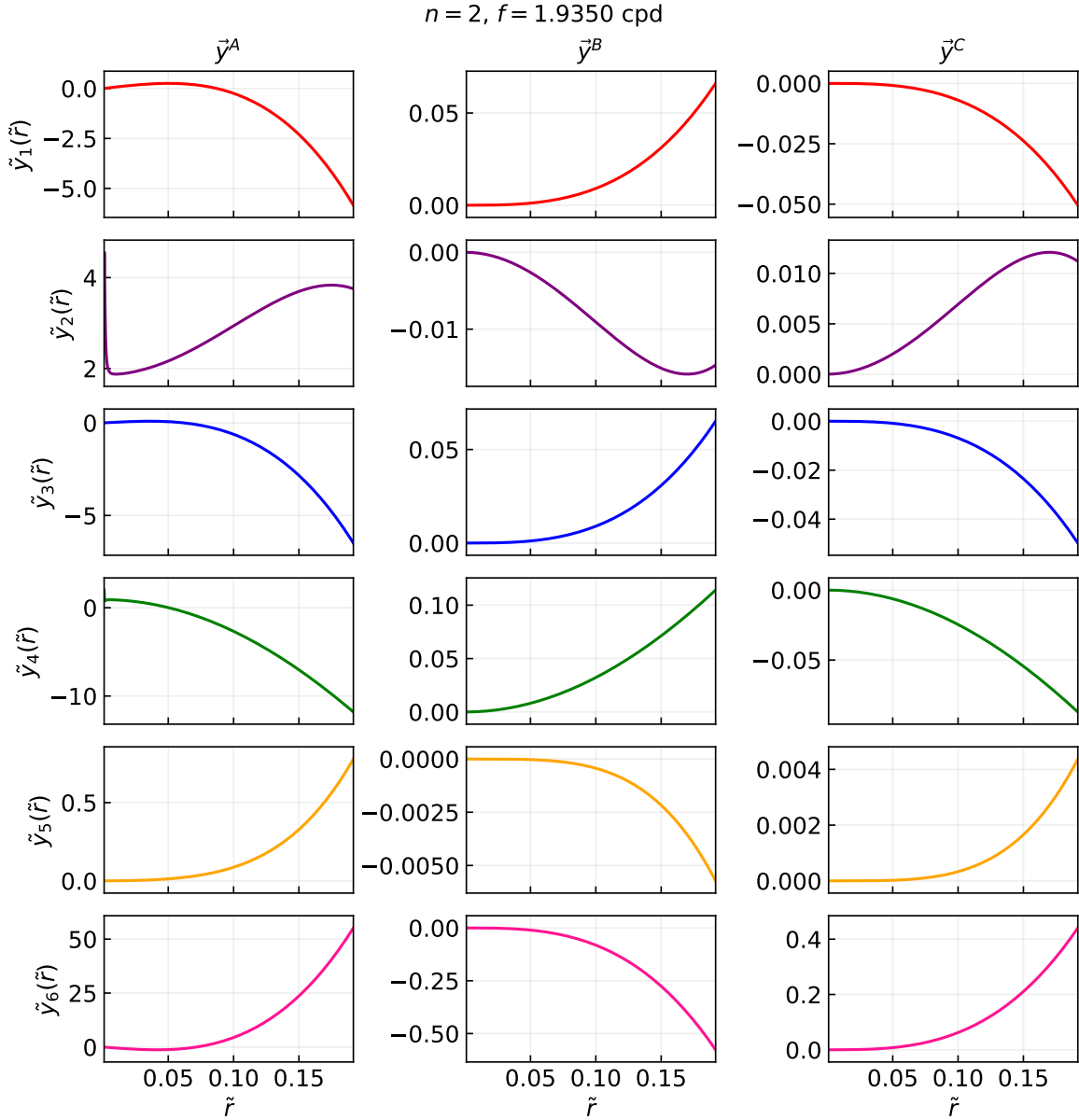


**Figure 5.7:** Integration of the radial functions  $y_i(r)$  through the Earth's inner core, from the initial radius  $r_0$  near the centre to the ICB, using the PREM density, gravity and elastic properties. Each column shows an independent set of solutions obtained from the power-series expansion at the centre, equations (4.33), and integrated using the system of first-order ODEs (4.18). From left to right, the columns represent the solutions  $\vec{y}^A$ ,  $\vec{y}^B$  and  $\vec{y}^C$ , respectively. The results are shown in dimensionless units.

$$\begin{aligned}
 z_1(c) &= Ay_1^A(c) + By_1^B(c) + Cy_1^C(c), && \text{(radial displacement)} \\
 z_2(c) &= Ay_2^A(c) + By_2^B(c) + Cy_2^C(c) = \rho(gz_1(c) - z_5(c)), && \text{(radial stress)} \\
 z_4(c) &= Ay_2^A(c) + By_2^B(c) + Cy_2^C(c) = 0 && \text{(tangential stress)} \\
 z_5(c) &= Ay_5^A(c) + By_5^B(c) + Cy_5^C(c), && \text{(gravitational potential)} \\
 z_6(c) &= Ay_6^A(c) + By_6^B(c) + Cy_6^C(c)
 \end{aligned} \tag{5.3}$$

This system of five equations has six unknowns:  $A$ ,  $B$ ,  $C$ ,  $z_1(c)$ ,  $z_5(c)$  and  $z_6(c)$ . This means we can't solve it completely. However, as we will now integrate the system of ODEs in equations (4.21), we can express the initial conditions,  $z_5(c)$  and  $z_7(c)$ , in terms of the remaining unknown coefficient,  $A$ . After some mathematical developments using equations (5.3), we found expressions for  $B$  and  $C$  in terms of  $A$  with the form:

$$\begin{aligned} B &= A \cdot V^A(z_i(c), \rho(c), g(c)), \\ C &= A \cdot S^A(z_i(c), \rho(c), g(c)) \end{aligned} \quad (5.4)$$

We performed this calculation using *Sympy* (Meurer et al., 2017) because the algebraic manipulations were lengthy. Finally,  $z_i(c)$  for  $i = 1, 5, 6$  can be written as:

$$z_i(c) = A\hat{z}_i(c) \quad (5.5)$$

$$= A [y_i^A(c) + V^A y_i^B(c) + S^A y_i^C(c)] \quad (5.6)$$

And  $z_7(c)$  as:

$$z_7(c) = A\hat{z}_7(c) \quad (5.7)$$

$$= A \left[ \hat{z}_6(c) + 4\pi G\rho(c)z_1(c) + \left( \frac{n+1}{c} - \frac{4\pi G\rho(c)}{g(c)} \right) z_5(c) \right] \quad (5.8)$$

Therefore, the  $\hat{z}_5(c)$  and  $\hat{z}_7(c)$  could serve as our initial conditions for the integration in the outer core.

7. **Integrate the ODEs in the outer core.** We proceed with the integration in the outer core, up to  $r = b$ , the CMB. Figure 5.8 shows the results of this integration for the PREM. In the end, we get global solutions of the form:

$$z_i(b) = A\hat{z}_i(b) \quad (5.9)$$

Following the  $z_7$  definition (equation (4.20)) and equations (4.22), these solutions must still satisfy:

$$\begin{aligned} z_2(b) &= \rho(g(b)z_1(b) - z_5(b)), \\ z_6(b) &= z_7(b) - 4\pi G\rho z_1(b) - \left( \frac{n+1}{b} - \frac{4\pi G\rho}{g(b)} \right) z_5(b), \\ z_4(b) &= 0 \end{aligned} \quad (5.10)$$

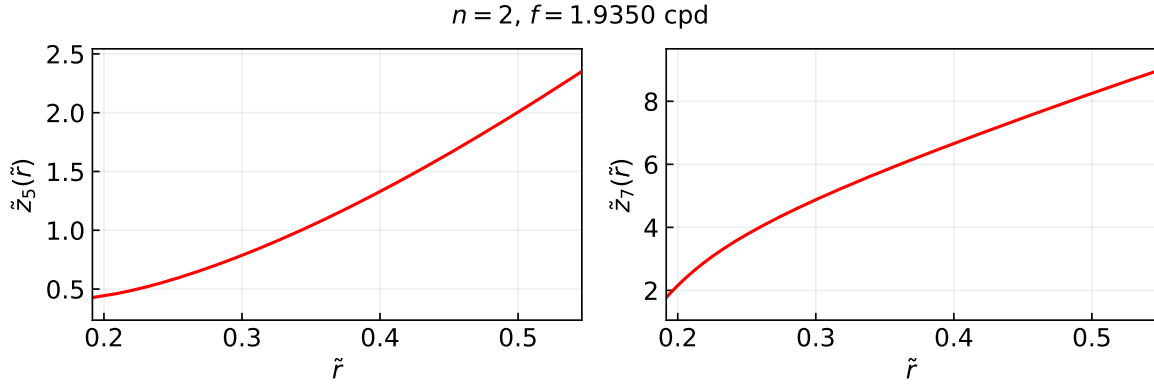


**Figure 5.8:** Integration of the radial functions  $z_i(r)$  through the Earth's outer core, from the ICB to the CMB, using the PREM density and gravity. The functions were obtained by the integration of the ODEs described in equations (4.21). The results are shown in dimensionless units.

8. **Define the initial solutions for the mantle.** For the mantle and crust, we return to the functions  $y_i(r)$ . Based on the global solutions at the CMB, we can define three independent solutions, each corresponding to one of the unknown coefficients  $A$ ,  $z_1(b)$  and  $y_3(b)$ :

$$\vec{y}^\alpha(b) = \begin{pmatrix} 0 \\ -\rho(b)\widehat{z}_5(b) \\ 0 \\ 0 \\ \widehat{z}_5(b) \\ \widehat{z}_7(b) - \left(\frac{n+1}{b} - \frac{4\pi G\rho(b)}{g(b)}\right)\widehat{z}_5(b) \end{pmatrix}, \quad (5.11)$$

$$\vec{y}^\beta(b) = \begin{pmatrix} 1 \\ \rho(b)g(b) \\ 0 \\ 0 \\ 0 \\ -4\pi G\rho(b) \end{pmatrix}, \quad \vec{y}^\gamma(b) = \begin{pmatrix} 0 \\ 0 \\ 1 \\ 0 \\ 0 \\ 0 \end{pmatrix}$$

That are combined to give the global solution at  $r = b$ :

$$\vec{y}(b) = A \cdot \vec{y}^\alpha(b) + z_1(b) \cdot \vec{y}^\beta(b) + \vec{y}^\gamma(b) \quad (5.12)$$

Vectors  $\vec{y}^\alpha(b)$ ,  $\vec{y}^\beta(b)$  and  $\vec{y}^\gamma(b)$  are then the initial conditions for the integration in the mantle.

9. **Integrate the ODEs in the mantle and crust.** The last integration corresponds to the region between the CMB and the Earth's surface at  $r = a_p$ . We integrate the mantle and crust together and don't separate them because the ODEs don't change between these two layers. We again use the ODEs in equations (4.18) for a solid region. Figure 5.9 shows the results of this integration for the PREM, with each column showing the components of one of the three independent solutions.
10. **Combine the final solutions.** Finally, to combine the solutions, we use the definitions of  $y_1$  and  $y_5$ , together with the boundary conditions at the surfaces (equations (4.24) and (4.27)). Let  $D = z_1(b)$  and  $E = y_3(b)$ . We then have the following system of equations:

$$\begin{aligned} Ay_1^\alpha(a_p) + Dy_1^\beta(a_p) + Ey_1^\gamma(a_p) &= y_1(a) \\ Ay_5^\alpha(a_p) + Dy_5^\beta(a_p) + Ey_5^\gamma(a_p) &= y_5(a) \\ Ay_2^\alpha(a_p) + Dy_2^\beta(a_p) + Ey_2^\gamma(a_p) &= 0 \\ Ay_4^\alpha(a_p) + Dy_4^\beta(a_p) + Ey_4^\gamma(a_p) &= 0 \\ Ay_6^\alpha(a_p) + Dy_6^\beta(a_p) + Ey_6^\gamma(a_p) + y_5 \frac{n+1}{a_p} &= \frac{2n+1}{a_p} \end{aligned} \quad (5.13)$$

Or in a matricial form:

$$\begin{pmatrix} y_1^\alpha(a_p) & y_1^\beta(a_p) & y_1^\gamma(a_p) & -1 & 0 \\ y_2^\alpha(a_p) & y_2^\beta(a_p) & y_2^\gamma(a_p) & 0 & 0 \\ y_4^\alpha(a_p) & y_4^\beta(a_p) & y_4^\gamma(a_p) & 0 & 0 \\ y_5^\alpha(a_p) & y_5^\beta(a_p) & y_5^\gamma(a_p) & 0 & -1 \\ y_6^\alpha(a_p) & y_6^\beta(a_p) & y_6^\gamma(a_p) & 0 & \frac{n+1}{a_p} \end{pmatrix} \begin{pmatrix} A \\ D \\ E \\ y_1(a) \\ y_5(a) \end{pmatrix} = \begin{pmatrix} 0 \\ 0 \\ 0 \\ 0 \\ \frac{2n+1}{a_p} \end{pmatrix} \quad (5.14)$$

This system comprises five equations and five unknowns and is inhomogeneous. Solving it yields the coefficients  $A$ ,  $D$  and  $E$ , as well as the values of  $y_1(a)$  and  $y_5(a)$  at the surface.

11. **Calculate the Love numbers.** Revisiting the definitions of the Love numbers in equations (4.4), we know that if we have the functions  $y_i(r)$ , we can estimate the Love numbers. As we conducted a dimensionless integration, i.e., we found  $\tilde{y}_i$  instead of  $y_i$ , we can directly write the Love numbers as:

$$h_n = \tilde{y}_1(1), \quad (5.15)$$

$$k_n = \tilde{y}_5(1) - 1, \quad (5.16)$$

$$l_n = A\tilde{y}_3^\alpha(1) + D\tilde{y}_3^\beta(1) + E\tilde{y}_3^\gamma(1) \quad (5.17)$$

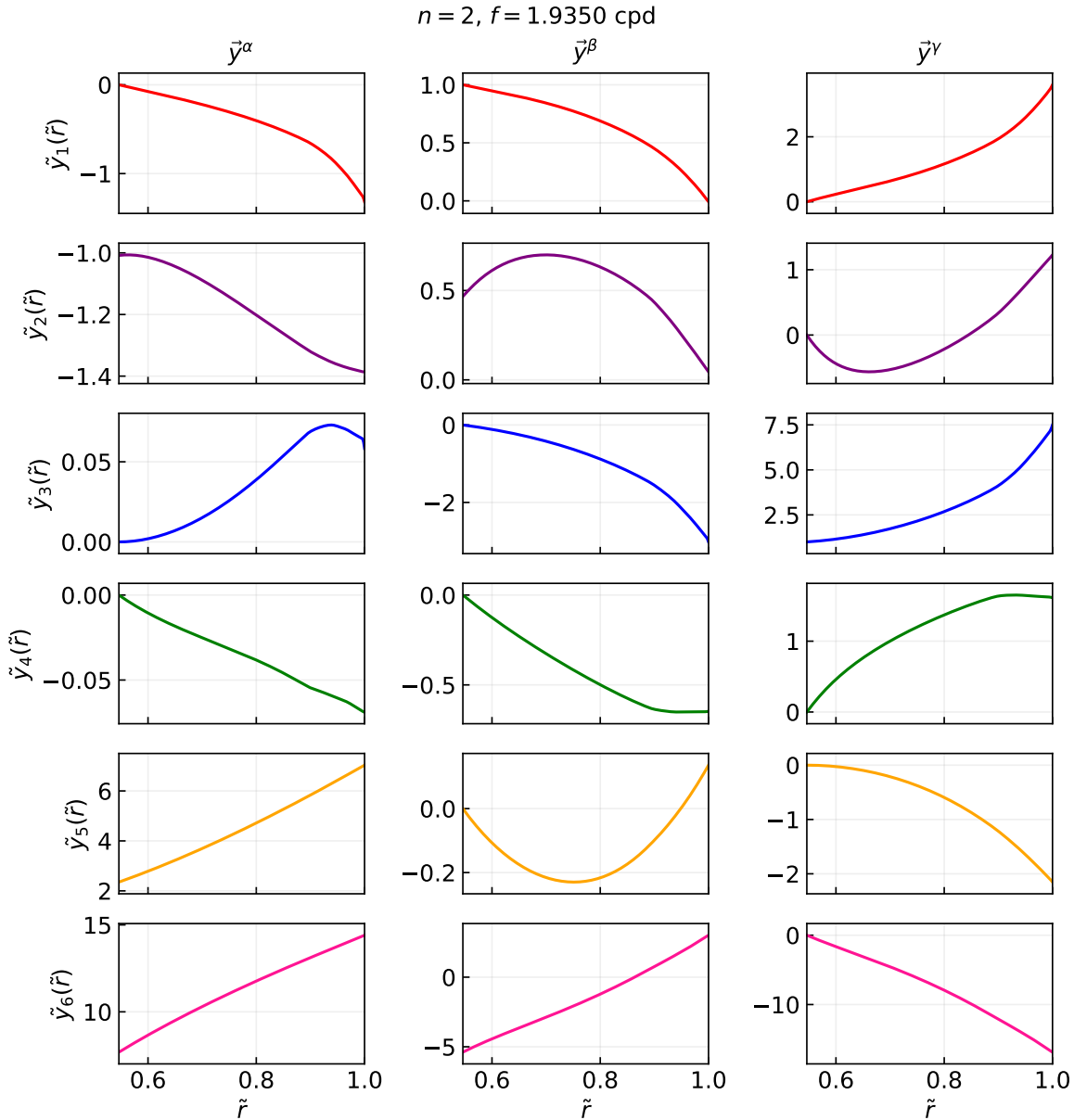


**Figure 5.9:** Integration of the radial functions  $y_i(r)$  through the Earth's mantle and crust, from the CMB to the planetary surface, using the PREM density, gravity and elastic parameters. Each column shows one of the three independent solutions defined at the CMB in equation(5.11):  $\vec{y}^\alpha$ ,  $\vec{y}^\beta$  and  $\vec{y}^\gamma$ . The integration uses the first-order ODEs system in equations (4.18). Results are shown in dimensionless units.

Because  $a_p$  is a unit in the dimensionless integration. Once again, this shows the convenience of using dimensionless quantities in the integration.

To test this scheme, we can compute the Earth's Love numbers across different frequencies and degrees, and compare them with other values found in the literature.

**Table 5.1:** Love numbers computed in this work, using the scheme from section 5.2.1 and TSPICE with the modified PREM at the  $M_2$  tidal frequency ( $f = 1.9323$  cpd), compared with values from Amorim & Gudkova (2024) and Xu & Sun (2003).

Love number	This work	AG <sup>a</sup>	Diff. AG (%)	XS <sup>b</sup>	Diff. XS (%)
$k_2$	0.29904	0.29872	0.11	0.29936	0.11
$h_2$	0.60931	0.60496	0.72	0.60563	0.61
$l_2$	0.08564	0.08399	1.96	0.08404	1.90
$k_3$	0.09285	0.09203	0.89	0.09216	0.75

<sup>a</sup>AG denotes Amorim & Gudkova (2024); <sup>b</sup>XS denotes Xu & Sun (2003).

### 5.2.2 Love numbers for the Earth

To validate the implementation of the integration scheme in section 5.2.1, we computed the Love numbers for the modified PREM at the principal lunar semidiurnal tide  $M_2$ , with frequency  $f = 1.9323$  cpd, following Amorim & Gudkova (2024). Table 5.1 presents our computed values alongside those reported by Amorim & Gudkova (2024) for the same model and frequency.

The computed Love numbers show excellent agreement with the reference values from Amorim & Gudkova (2024), with all differences below 2%. The degree-2 Love numbers, particularly  $k_2$ , show the best agreement, with a relative difference of only 0.11%. The parameters  $h_2$  and  $k_3$  differ by 0.72% and 0.89%, respectively, while  $l_2$  exhibits the largest relative difference at 1.96%. These small discrepancies are well within acceptable bounds for geophysical applications and may reflect minor numerical variations in the integration process, such as differences in step size, integration tolerance, and planetary model interpolation, rather than methodological errors.

Xu & Sun (2003) also integrated the coupled ODEs for the PREM at several tidal frequencies, but their description of the numerical setup (boundary conditions, step control and layer interpolation) omits some details. Our comparison therefore relies on their tabulated  $M_2$  values, which overlap with those reported by Amorim & Gudkova (2024). At that common frequency, our results also differ from Xu & Sun (2003) by less than 2%.

These results demonstrate that we correctly implemented the integration scheme of Amorim & Gudkova (2024) and that the classes and routines in TSPICE reliably reproduce, with good agreement, at least for the band around the  $M_2$  frequencies, the Love number values reported in the literature.

## 5.3 TSPICE: Tidal Signal with Python and SPICE

*TSPICE*, is a Python package developed in this work to facilitate the calculation of the tidal potential and the planetary response. The package incorporates the routine and the integration setup we described in section 5.1.1 and section 5.2.1. It is already available on PyPI, so you can install it easily with:

```
pip install tspice
```

After this, you can start using the package after importing it:

```
import tspice
```

Once the package is installed and imported into your script, you should run the following before you start using it:

```
tspice.initialize()
```

This downloads and loads the necessary SPICE kernels from the NAIF website. Internally, `initialize` looks for the kernels in the package's structure, and if they don't exist, it loads them with `furnsh`. If the kernels and the structure where they are stored don't exist, this function downloads them, creates the structure in the package folder, and loads them. Thus, the second time you use TSPICE, `initialize` won't download the kernels again. This guarantee step 1 from section 5.1.1 before any calculation.

In general, the package follows an object-oriented programming (OOP) paradigm, with the `Body` class as the most important. First, this class provides the methods required to compute the TGP. Because calculating the planetary response is more complex, requires additional physical information, and may not always be feasible, we create a second class, `BodyResponse`, that inherits the attributes and methods of `Body` and adds routines to compute the elastic response of the bodies to tides. We now describe the functionality of each of these classes.

### 5.3.1 Body class

The `Body` class encapsulates the information and methods required to compute the tidal potential for any target body. When instantiated, it retrieves and computes the key parameters of that body from the SPICE kernels, including the gravitational parameter  $GM$ , the mean radius  $a_p$ , the flattening  $f$ , and the reference gravity  $g$ . It provides the following helper methods to complete the routine in section 5.1.1:

- `array_et_utc`: Converts a dictionary containing time information in UTC to an array of ET formats. The dictionary should include the keys for the initial date, final date, and time step of the signal.
- `Kn_func`: Evaluates the degree-dependent scaling coefficient,  $K_n(a_p)$ , for a given harmonic degree  $n$ , given the body's physical parameters and the mass of the external body.
- `subpoint_coordinates`: Obtains the geographical coordinates of the sub-point,  $\theta'$  and  $\phi'$ , where an external body appears on the target body. To use it, we just need to specify the external body and the time in ET.
- `tgp_one_body`: This is the main routine that follows the workflow in section 5.1.1 to compute  $V_{\text{tid}}/g$  for a single external body. It uses the previous

routines to complete some steps and receives the location on the target body in latitude and longitude, the dictionary containing the time information, the name of the external body, and the  $n_{\max}$  required to compute the signal.

- `tgp_many_bodies`: Aggregates tidal potential contributions from multiple external bodies into a total signal. Internally, it runs `tgp_one_body` for each body and sums the contributions. It accepts essentially the same inputs as `tgp_one_body`, but with a list of external bodies rather than a single one.

Together, these methods provide a reproducible, modular pathway from the SPICE kernels to the tidal potential values.

### 5.3.2 BodyResponse class

As we mentioned, the `BodyResponse` class inherits from `Body` and extends it with methods for modelling the elastic response of Earth-like planets. The class is designed to compute Love numbers by integrating the coupled system of ODEs for a planetary model, initially using the scheme described in section 5.2.1. It is easy to incorporate new integration schemes in the future thanks to its modular structure, and it provides the following additional methods:

- `scale_constants`: Computes and stores the characteristic scale factors used to convert the physical parameters into dimensionless quantities, as described in step 2 of section 5.2.1. These scales include length ( $a_p$ ), mass ( $M_p$ ), density ( $\rho_0$ ), pressure ( $P_0$ ), gravity ( $g_0$ ), velocity ( $V_0$ ), time ( $T_0$ ), and angular frequency ( $\omega_0$ ). This method can optionally print the computed scales for verification purposes.
- `read_layers`: Processes the planetary model's layer structure to prepare it for integration. Given a list of layer dictionaries, this method sorts the layers from the centre outward, determines the number of integration steps per layer, and determines the corresponding step sizes. It also validates the layer order to ensure consistency with the integration requirements. Each dictionary in the input list should specify the layer name, the type (i.e. solid or fluid), and radial boundaries (the radii of both boundaries). The method returns the sorted layer list along with dictionaries containing the number of steps and step sizes for each layer.
- `set_integration_parameters_ad`: Configures all parameters required for the numerical integration of the ODEs in dimensionless form. This includes setting the harmonic degree  $n$ , the harmonic frequency (provided in cycles per day, cpd, and converted to dimensionless angular frequency), the list of the layer structure (the same as in `read_layers`), and a dictionary of the planetary profile functions (density, gravity, and elastic parameters as functions of radius). The dictionary of the planetary profile functions can also specify whether the functions are already dimensionless. Additionally, the method requires the initial radius  $r_0$  from which integration begins. The

method doesn't return anything, but it stores all the parameters as attributes of the class instance, making them accessible to subsequent integration routines.

- `initial_conditions_ad`: Computes the dimensionless initial conditions for the three independent solutions at the centre of the planet using the power series expansions described in equation (4.33). The method returns three arrays, corresponding to the independent solutions ( $\vec{y}^{A0}$ ,  $\vec{y}^{B0}$ , and  $\vec{y}^{C0}$ ), which serve as starting points for the numerical integration.
- `integrate_internal_solutions_ad`: Executes the complete integration routine across all planetary layers, from the initial radius  $r_0$  to the surface. This method follows the integration scheme outlined in section 5.2.1, handling transitions between solid and fluid layers, applying the appropriate boundary conditions at each interface, and combining the independent solutions. The method can optionally print progress information during integration. Upon completion, it stores the radial functions  $y_i(r)$  at the surface and computes the Love numbers using equation (4.4). The Love numbers and other relevant integration results are stored as attributes for later retrieval. Hence, it is the most important method in the class, but it requires `set_integration_parameters_ad` to be run beforehand.

The package includes additional utility scripts that support both `Body` and `BodyResponse`, providing common helpers and simple visualisation routines. Specific scripts also include sets of ODEs for solid and fluid layers, along with helper functions to construct the initial conditions used by `BodyResponse`. This separation keeps the class focused on orchestration while allowing the underlying equations and auxiliary tools to be maintained independently. Moreover, although the current implementation follows the proposal of Amorim & Gudkova (2024), the design was intended to accommodate future alternative integration setups, so that TSPICE can be extended to handle additional planetary models without changing the user-facing API.

### 5.3.3 Examples

The following example shows how to use TSPICE in a Python script to compute the TGP on a body, in this case the Earth, due to a list of external bodies at a specific location over a specified time range. It assumes you have already installed TSPICE.

```

1 # Import TSPICE and initialize the kernels
2 import tspice
3 tspice.initialize()
4
5 # Create the Body object for the Earth
6 earth = tspice.Body('Earth')
7
8 # Coordinates of the station in radians
9 loc = dict(lat = 4.49,
10             lon = -73.14,
```

```

11         depth = 9)
12
13 #Dictionary with the start, stop, and step data
14 date = dict(start = '2025-05-25 13:08:05',
15             stop = '2025-06-22 13:08:05',
16             step = '1h',
17             time_frame = 'UTC')
18
19 #List of bodies to consider for tidal calculations
20 bodylist = ['Moon', 'Sun', 'Mercury', 'Venus', 'Mars', 'Jupiter']
21
22 #Get the tidal potential due just to the Moon
23 tgp, et_times = earth.tgp_many_bodies(bodylist, loc_sta=loc, dates=date, nmax=6, ←
24     time_array=True, verbose=True)
25
26 #Plotting the signal
27 tspice.plot_one_signal(et_times, tgp*100, loc=loc, colors=['blue', 'red'], mean_value=True←
28 )

```

We also include an example of how to use TSPICE to compute the Earth's Love numbers for a given tidal frequency and degree. Again, it assumes you have already installed TSPICE and have access to the planetary model functions, in this case the modified PREM.

```

1 #Import TSPICE and initialize the kernels
2 import tspice as tsp
3 tsp.initialize()
4
5 #Uploading the PREM model
6 from data.prem import prem_amorim as prem
7
8 #Define the planet profiles
9 planet_profile = {'rho': prem.rho_r_interp,
10                   'lamb': prem.lamb_r_interp,
11                   'mu': prem.mu_r_interp,
12                   'g': prem.g_r_interp,
13                   'dimensionless': False}
14
15 #Create the BodyResponse object for the Earth
16 earth_interior = tsp.BodyResponse('Earth')
17
18 #Define layers for our planetary model
19 earth_interior.scale_constants(verbose=True)
20 layers_list = [dict(name='Outer Core', type='fluid', r0=1221500.0, rf=3480000.0),
21                 dict(name='Inner Core', type='solid', r0=0, rf=1221500.0),
22                 dict(name='Mantle + crust', type='solid', r0=3480000.0, rf = ←
23                     earth_interior.L)]
24
25 #Set parameters for the integration
26 n = 2
27 f_cpd = 1.93502 #M2 tide in cpd
28 r0_ini = 6e3
29 earth_interior.set_integration_parameters_ad(n=n, f_days=f_cpd, layers_list=layers_list, ←
30     planet_profile=planet_profile, r0_ini=r0_ini)
31
32 #Integration
33 earth_interior.integrate_internal_solutions_ad(verbose=True)
34
35 #After the integration, we can get the Love numbers as attributes
36 print(f'k_{n}({f_cpd}) = {earth_interior.k_n}')

```

# 6 . Analysis & Future Work

# 7. Conclusions

# A . Appendix: SPICE

# Bibliography

- Acton, C., Bachman, N., Semenov, B., & Wright, E. 2018, Planetary and Space Science, 150, 9, doi: [10.1016/j.pss.2017.02.013](https://doi.org/10.1016/j.pss.2017.02.013)
- Acton, C. H. 1996, Planetary and Space Science, 44, 65, doi: [10.1016/0032-0633\(95\)00107-7](https://doi.org/10.1016/0032-0633(95)00107-7)
- Agnew, D. 2015, Earth Tides, second edition edn., ed. G. Schubert (Oxford: Elsevier), 151–178, doi: [10.1016/B978-0-444-53802-4.00058-0](https://doi.org/10.1016/B978-0-444-53802-4.00058-0)
- Altermann, Z., Jarosch, H., & Pekeris, C. L. 1959, Proceedings of the Royal Society of London. Series A. Mathematical and Physical Sciences, 252, 80, doi: [10.1098/rspa.1959.0138](https://doi.org/10.1098/rspa.1959.0138)
- Amorim, D. O., & Gudkova, T. 2024, Physics of the Earth and Planetary Interiors, 347, 107144, doi: <https://doi.org/10.1016/j.pepi.2024.107144>
- . 2025, Physics of the Earth and Planetary Interiors, 359, 107304, doi: <https://doi.org/10.1016/j.pepi.2024.107304>
- Annex, A. M., Pearson, B., Seignovert, B., et al. 2020, Journal of Open Source Software, 5, 2050, doi: [10.21105/joss.02050](https://doi.org/10.21105/joss.02050)
- Astropy Collaboration, Robitaille, T. P., Tollerud, E. J., et al. 2013, A&A , 558, A33, doi: [10.1051/0004-6361/201322068](https://doi.org/10.1051/0004-6361/201322068)
- Astropy Collaboration, Price-Whelan, A. M., Sipőcz, B. M., et al. 2018, AJ , 156, 123, doi: [10.3847/1538-3881/aabc4f](https://doi.org/10.3847/1538-3881/aabc4f)
- Astropy Collaboration, Price-Whelan, A. M., Lim, P. L., et al. 2022, ApJ , 935, 167, doi: [10.3847/1538-4357/ac7c74](https://doi.org/10.3847/1538-4357/ac7c74)
- Cartwright, D. E., & Tayler, R. J. 1971, Geophysical Journal International, 23, 45, doi: [10.1111/j.1365-246x.1971.tb01803.x](https://doi.org/10.1111/j.1365-246x.1971.tb01803.x)
- Chinnery, M. A. 1975, Geophysical Journal of the Royal Astronomical Society, 42, 461 – 475., doi: [10.1111/j.1365-246x.1975.tb05872.x](https://doi.org/10.1111/j.1365-246x.1975.tb05872.x)

- Crossley, D. J. 1975, Geophysical Journal International, 41, 153, doi: [10.1111/j.1365-246x.1975.tb04145.x](https://doi.org/10.1111/j.1365-246x.1975.tb04145.x)
- Deparis, V., Legros, H., & Souchay, J. 2013, Investigations of Tides from the Antiquity to Laplace, ed. J. Souchay, S. Mathis, & T. Tokieda (Berlin, Heidelberg: Springer Berlin Heidelberg), 31–82, doi: [10.1007/978-3-642-32961-6\\_2](https://doi.org/10.1007/978-3-642-32961-6_2)
- Dziewonski, A. M., & Anderson, D. L. 1981, Physics of the Earth and Planetary Interiors, 25, 297, doi: [https://doi.org/10.1016/0031-9201\(81\)90046-7](https://doi.org/10.1016/0031-9201(81)90046-7)
- Ginsburg, A., Sipőcz, B. M., Brasseur, C. E., et al. 2019, AJ, 157, 98, doi: [10.3847/1538-3881/aafc33](https://doi.org/10.3847/1538-3881/aafc33)
- Greff-Lefftz, M., Métivier, L., & Legros, H. 2005, Celestial Mechanics and Dynamical Astronomy, 93, 113, doi: [10.1007/s10569-005-6424-3](https://doi.org/10.1007/s10569-005-6424-3)
- Hartmann, T., & Wenzel, H. 1995, Geophysical Research Letters, 22, 3553, doi: [10.1029/95gl03324](https://doi.org/10.1029/95gl03324)
- Jaeger, J. C., Cook, N. G., & Zimmerman, R. W. 2007, Fundamentals of Rock Mechanics, 4th edn., Blackwell Publishing (Malden, MA: Blackwell Publishing)
- Lainey, V., Zannoni, M., Robert, V., & Guillot, T. 2025, Space Science Reviews, 221, 93
- Lautrup, B. 2011, Physics of continuous matter (CRC Press), doi: [10.1201/9781439894200](https://doi.org/10.1201/9781439894200)
- Longman, I. M. 1963, Journal of Geophysical Research (1896–1977), 68, 485, doi: <https://doi.org/10.1029/JZ068i002p00485>
- Love, A. E. H. 1911, Some Problems of Geodynamics (Cambridge University Press)
- . 1944, A Treatise on the Mathematical Theory of Elasticity, 4th edn. (New York: Dover Publications)
- Meurer, A., Smith, C. P., Paprocki, M., et al. 2017, PeerJ Computer Science, 3, e103, doi: [10.7717/peerj-cs.103](https://doi.org/10.7717/peerj-cs.103)
- Michel, A., & Boy, J. 2021, Geophysical Journal International, 228, 1191, doi: [10.1093/gji/ggab369](https://doi.org/10.1093/gji/ggab369)
- Saito, M. 1974, Journal of Physics of the Earth, 22, 123, doi: [10.4294/jpe1952.22.123](https://doi.org/10.4294/jpe1952.22.123)
- Schueller, K. 2020, Program System ETERNA-x et34-x-v80 for Earth and Ocean Tides Analysis and Prediction, Research Initiative for Tidal Analysis (RITA), Surin Province, Thailand
- Sepúlveda, A. 2004, Lecciones de Física Matemática, 2nd edn. (Medellín)

- Shida, T. 1912, Proceedings of the Tokyo Mathematico-Physical Society. 2nd Series, 6, 242, doi: [10.11429/ptmps1907.6.16\\_242](https://doi.org/10.11429/ptmps1907.6.16_242)
- Simon, B., Lemaitre, A., & Souchay, J. 2013, Oceanic Tides, ed. J. Souchay, S. Mathis, & T. Tokieda (Berlin, Heidelberg: Springer Berlin Heidelberg), 83–114, doi: [10.1007/978-3-642-32961-6\\_3](https://doi.org/10.1007/978-3-642-32961-6_3)
- Takeuchi, H., & Saito, M. 1972, in Methods in Computational Physics: Advances in Research and Applications, Vol. 11, Seismology: Surface Waves and Earth Oscillations, ed. B. A. Bolt (Elsevier), 217–295, doi: <https://doi.org/10.1016/B978-0-12-460811-5.50010-6>
- Tokieda, T. 2013, Tides: A Tutorial, ed. J. Souchay, S. Mathis, & T. Tokieda (Berlin, Heidelberg: Springer Berlin Heidelberg), 1–30, doi: [10.1007/978-3-642-32961-6\\_1](https://doi.org/10.1007/978-3-642-32961-6_1)
- Unterborn, C. T., Dismukes, E. E., & Panero, W. R. 2016, The Astrophysical Journal, 819, 32, doi: [10.3847/0004-637x/819/1/32](https://doi.org/10.3847/0004-637x/819/1/32)
- VanderPlas, J. T. 2018, The Astrophysical Journal Supplement Series, 236, 16, doi: [10.3847/1538-4365/aab766](https://doi.org/10.3847/1538-4365/aab766)
- van Dijk, E. A., & Miguel, Y. 2025, Monthly Notices of the Royal Astronomical Society, 540, 1544, doi: [10.1093/mnras/staf814](https://doi.org/10.1093/mnras/staf814)
- Varga, P., & Grafarend, E. 2018, Geodynamics and Earth tides observations from global to micro scale, 55
- Virtanen, P., Gommers, R., Oliphant, T. E., et al. 2020, Nature Methods, 17, 261, doi: [10.1038/s41592-019-0686-2](https://doi.org/10.1038/s41592-019-0686-2)
- Wenzel, H.-G. 1996, Bull. Inf. Marées Terrestres, 124, 9425
- Xu, J., & Sun, H. 2003, Chinese Journal of Geophysics, 46, 465, doi: [10.1002/cjg2.3364](https://doi.org/10.1002/cjg2.3364)
- Yan, R., Chen, X., Sun, H., Xu, J., & Zhou, J. 2023, Geodesy and Geodynamics, 14, 35, doi: <https://doi.org/10.1016/j.geog.2022.06.005>